WHITBY ABBEY CLIFF, WHITBY, NORTH YORKSHIRE:
Archaeomagnetic Dating Report 2001

Paul Linford

Summary

During excavations on the cliff top at Whitby Abbey in North Yorkshire, a number of fired clay features were discovered. These features were thought to relate to the settlement associated with the original abbey in the Anglo-Saxon and Anglo-Scandinavian periods. Four were sampled for archaeomagnetic dating to help establish a chronology for the site. Three of these were associated with a rectangular area of indeterminate function delineated by a masonry kerb. Archaeomagnetic analysis demonstrated that this feature was most probably last fired during the 8th Century AD. Dating of the fourth feature indicated that there had still been activity on the site some 250 years later.

WHITBY ABBEY CLIFF, WHITBY, NORTH YORKSHIRE:
Archaeomagnetic Dating Report 2001

Introduction

During excavations on the cliff top at Whitby Abbey in North Yorkshire (NZ 904 114, longitude 0.6°W, latitude 54.5°N), carried out by Peter Buzby of the English Heritage Centre for Archaeology (C*f*A) in 2001, a number of fired clay features were discovered. These were thought to relate to the settlement associated with the original abbey in the Anglo-Saxon and Anglo-Scandinavian periods. However, it was also possible that the remains dated from the Roman or early post-Roman eras. Four burnt surface features were sampled for archaeomagnetic dating and given the codes 1WB to 4WB.

Three of these features (1WB, 3WB and 4WB) lay within a rectangular area of indeterminate function, delineated by a kerb of masonry blocks (Figure 1, left). Features 1WB and 3WB (archaeological contexts 30980 and 39201) appeared to be successive resurfacings of a smoothed clay floor upon which a fire was set. The uppermost surface, 1WB, had imprints of plant fibres indented into it. The remaining floor within the kerbed area appeared to be natural soil, which had been reddened by heat in places. Three patches that had become well magnetised by this heating were sampled as feature 4WB (archaeological context 39211). A fourth feature, 2WB (archaeological context 30985) lay outside the rectangular kerb and appeared to be a deposit of clay and sandstone that had been heated *in situ* and possibly formed the base of a fire. It overlay an earlier ditch fill.

All archaeomagnetic sampling was carried out between the 25th and 27th of July 2001 by the author who also performed the subsequent laboratory measurement and analysis.

Method

Samples were collected using the disc method (see appendix, section 1a). Samples from feature 1WB were orientated to true north using a gyro-theodolite. The samples from the other features were orientated using a magnetic compass, the deviation between magnetic and true north in the area having been established when the gyro-theodolite was used.

The natural remanent magnetisation (NRM) measured in archaeomagnetic samples is assumed to be caused by thermoremanent magnetisation (TRM) created at the time when the feature of which they were part was last fired. However, a secondary component acquired in later geomagnetic fields can also be present, caused by diagenesis or partial reheating. Additionally, the primary TRM may be overprinted by a viscous component, depending on the grain size distribution within the magnetic material. These secondary components are usually of lower stability than the primary TRM and can thus be removed by partial demagnetisation of the samples.

A typical strategy for analysing a set archaeomagnetic samples from a fired archaeological feature is to first measure their NRM magnetisation. These NRM measurements are then

inspected and one or more samples are selected for pilot partial demagnetisation. Pilot demagnetisation of a sample involves exposing it to an alternating magnetic field of fixed peak strength and measuring the resulting changes in its magnetisation. The procedure is repeated with increasing peak field strengths to build up a complete picture of the coercivity spectrum of the pilot sample. From these pilot partial demagnetisation results an optimum peak field strength is selected to be applied to the remaining samples. This optimum field strength is chosen to remove as much of the secondary magnetisation as possible whilst leaving the primary magnetisation intact. The equipment used for these measurements is described in section 2 of the appendix.

A mean TRM direction is then calculated from the partially demagnetised sample measurements. Some samples may be excluded from this calculation if their TRM directions are so anomalous as to make them statistical outliers from the overall TRM distribution. A "magnetic refraction" correction is often applied to the sample mean TRM direction to compensate for distortion of the earth's magnetic field due to the geometry of the magnetic fabric of the feature itself. Then the mean is adjusted according to the location of the feature relative to a notional central point in the UK (Meriden), so that it can be compared with UK archaeomagnetic calibration data to produce a date of last firing for the feature. Notes concerning the mean calculation and subsequent calibration can be found in sections 3 and 4 of the appendix.

This measurement and calibration strategy was applied to the analysis of the samples from the Whitby Cliff excavation. As all the samples were taken from the floors of features, a magnetic refraction correction (Aitken and Hawley, 1971) of 2.4^{o} was added to the inclination of each mean TRM direction before calibration.

Results

Table 1 summarises the mean TRM directions and the inferred date ranges for all the features sampled at the Whitby Headland excavation. The following text provides descriptions of the features sampled and notes any important points about their archaeomagnetic analysis. TRM measurements for all samples may be found grouped by feature in the tables at the end of the report. These tables also record each sample's composition, the demagnetisation level applied to it and whether it was rejected from the feature's mean TRM calculation.

Feature	N	Dec°	Inc°	α_{95}	k	Date Range	Description
1WB (context 30980)	18	6.9 (6.8)	77.2 (75.9)	1.8	390.3	63%: 685 – 795 AD 95%: 590 – 810 AD	Very well baked clay surface with impressions of plant fibres in corner of kerbed area.
2WB (context 30985)	7	30.4 (28.9)	69.6 (68.1)	3.6	277.6	63%: 980 – 1045 AD 95%: 920 – 1085 AD (or 600 – 400 BC)	Area of fired clay and reddened sandstone above earlier ditch fill.
3WB (context 39201)	10	22.9 (21.7)	75.6 (74.3)	3.1	246.0	63%: not datable 95%: 560 – 850 AD (or 535 – 200 BC)	Earlier surface beneath 1WB.
4WB (context 39211)	13	6.8 (6.7)	76.3 (75.1)	2.5	268.0	63%: 615 – 800 AD 95%: 560 – 825 AD	Burnt clay patches in kerbed area that contained features 1WB and 3WB.
1+4WB	31	6.9 (6.8)	76.8 (75.6)	1.4	336.8	63%: 730 – 790 AD 95%: 605 – 805 AD	Mean of samples from both 1WB and 4WB, assuming the two are contemporary.

Table 1; Archaeomagnetic dates inferred for features from the Whitby Headland excavation. N = number of samples used to calculate mean TRM. Dec = mean declination (bracketed value is Meriden corrected). Inc = mean inclination (bracketed value is Meriden corrected). α_{95} = internal angle of cone of confidence. k = Fisher precision statistic.

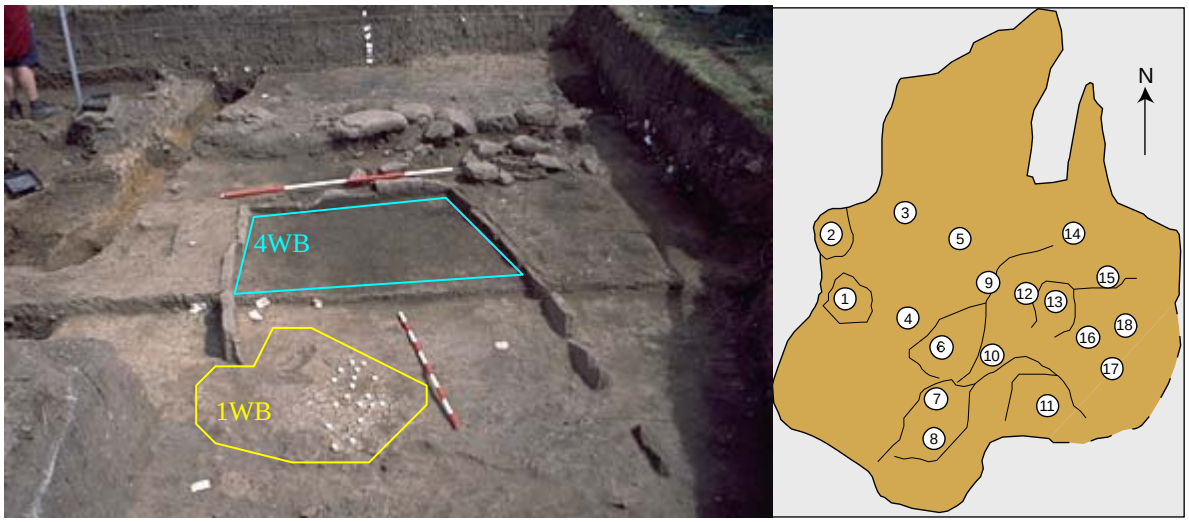

Figure 1. Left: Photograph of feature 1WB (foreground) during sampling, viewed from the north. The stone kerb and the burnt soil feature 4WB can be seen in the background. Right: Sketch plan showing distribution of samples taken from 1WB (not to scale).

Feature 1WB (context 30980)

This was a hearth-like surface composed of extremely well baked yellow clay, cracked in places. On close inspection impressions of plant fibres were visible in the clay. Approximate sample locations are depicted in Figure 1 and sample measurements are recorded in Tables 2 and 3. Figure 6 depicts the distribution of sample TRM directions before and after partial demagnetisation. Figures 7 and 8 illustrate the results of pilot demagnetisation on samples 1WB05 and 1WB16 respectively. The magnetisation in both samples was extremely stable with a small viscous component apparent in coercivities below 5mT. Some very slight alteration in the magnetisation directions was noted in demagnetisation steps up to 10mT, so this field strength was chosen to partially demagnetise the remaining samples. Figure 9 shows the comparison between the mean TRM direction calculated from all the samples and the UK archaeomagnetic calibration curve.

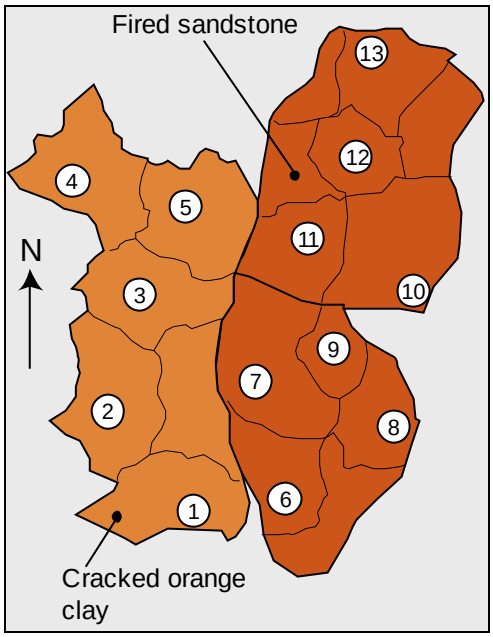

Figure 2: Sketch plan showing distribution of samples taken from feature 2WB (not to scale).

Feature 2WB (context 30985)

This feature appeared to be an area of *in situ* burning composed of reddened clay and sandstone overlying an earlier ditch fill a few metres to the west of feature 1WB. Approximate sample locations are depicted in Figure 2 and sample measurements are recorded in Tables 4 and 5. Figure 10 depicts the distribution of sample TRM directions before and after partial demagnetisation. It is immediately clear from Figure 10a that the NRM directions of the clay samples 2WB01-05 are widely scattered. This may be due to disturbance since firing, or perhaps because this area was shielded from direct heat by another piece of stone that was subsequently removed. It was decided that these samples would not provide a reliable record of the direction of the Earth's magnetic field at the time the feature was last fired and they were not analysed further.

Figures 11 and 12 illustrate the results of pilot demagnetisation on sandstone samples 2WB09 and 2WB10 respectively. The magnetisation in sample 2WB09 was extremely weak and some of the instability apparent in Figure 11 may in fact be due to instrument noise. The magnetisation in 2WB10 was far stronger than in any of the other sandstone samples and the

magnetisation direction appeared stable. A 5mT field was chosen to partially demagnetise the remaining samples, as a small viscous component was apparent at low coercivities. After partial demagnetisation the TRM direction of sample 2WB10 was still anomalous. This is probably due to magnetic distortion caused by the anomalously high magnetisation per unit volume in this sample. 2WB10 was thus rejected from the mean calculation as well as the clay samples. Figure 13 shows the comparison between the mean TRM direction calculated from the remaining seven sandstone samples and the UK archaeomagnetic calibration curve.

Figure 3. Left: Photograph of surface 3WB view from the southeast. Surface 1WB can be seen overlying it at the top left of the frame. Right: Sketch plan showing distribution of samples (not to scale).

Feature 3WB (context 39201)

This feature was a second, earlier, surface lying beneath feature 1WB. Approximate sample locations are depicted in Figure 3 and sample measurements are recorded in Tables 6, 7 and 8. Figure 14 depicts the distribution of sample TRM directions before and after partial demagnetisation. Figures 15 and 16 illustrate the results of pilot demagnetisation on samples 3WB05 and 3WB10 (samples 3WB02 and 3WB13 were also demagnetised with results similar to those of 3WB10 and 3WB05 respectively). The magnetisation directions of these samples were extremely stable with some viscous realignment in domains with coercivities below 5mT. Hence the remaining samples were partially demagnetised in a 5mT AF field. Samples 3WB02, 3WB04-5 and 3WB07 exhibited TRM inclinations somewhat steeper than the maximum recorded in the UK Archaeomagnetic Calibration Database for the past 3000 years. It is likely that this is because these samples were from areas that had been disturbed either in antiquity when this clay floor was resurfaced, or during excavation. For this reason they were excluded from the mean TRM calculation. Figure 17 shows the comparison of the calculated mean TRM vector with the UK archaeomagnetic calibration curve.

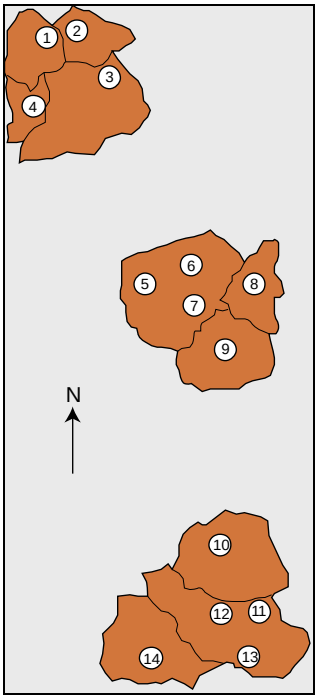

Figure 4: Sketch plan showing distribution of samples taken from feature 4WB (not to scale).

Feature 4WB (context 39211)

This feature consistent of a group of patches of burnt clay within the rectangular stone kerbed area that also contained feature 1WB. 4WB appeared to be natural soil forming the floor of this area. Three well reddened areas were sampled as depicted in Figure 4. Sample measurements are recorded in Tables 9 and 10. Figure 18 depicts the distribution of sample TRM directions before and after partial demagnetisation. Figures 19 and 20 illustrate the results of pilot demagnetisation on samples 4WB02 and 4WB11 respectively (pilot demagnetisation was also carried out on sample 4WB08 with similar results). The magnetisation directions of these samples were stable with some viscous realignment in domains with coercivities below 5mT. Hence the remaining samples were partially demagnetised in a 5mT AF field. Sample 4WB11 exhibited an anomalous magnetisation direction compared to the other samples, perhaps due to magnetic distortion caused by its much higher magnetisation intensity. It was excluded from the mean TRM calculation. Figure 21 shows the comparison of the calculated mean TRM vector with the UK archaeomagnetic calibration curve.

Conclusions

Archaeomagnetic analysis of the four features from Whitby has demonstrated that they have all acquired stable TRMs as a result of heating in the past. Date ranges have been inferred for the last firing of the features and these are quoted in Table 1 and depicted graphically in Figure 5.

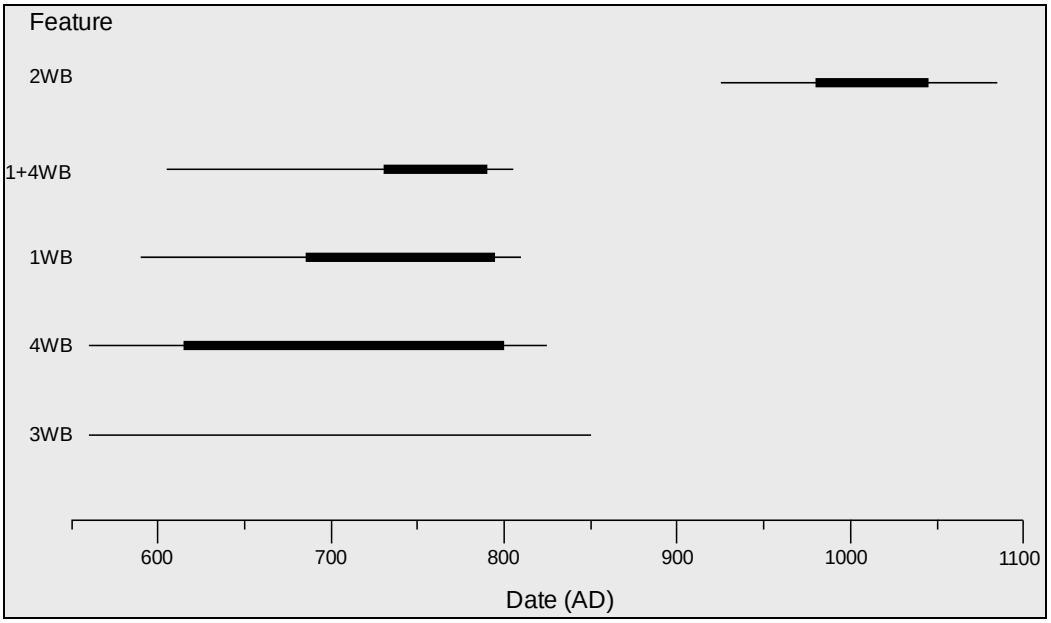

Figure 5: Archaeomagnetic date ranges of features from Whitby Abbey Cliff. Thin lines represent 95% confidence intervals, thick lines represent 63% confidence intervals. 1+4WB is the mean of samples from both 1WB and 4WB on the assumption that these two features are contemporary.

Unfortunately the mean TRM direction of feature 3WB lies some distance from any segment of the UK Archaeomagnetic Calibration Curve, and it is not possible to infer a date range at the 63% confidence level. Furthermore, it should be noted that, at the 95% confidence level, features 2WB and 3WB also have possible archaeomagnetic date ranges in the Iron Age and these have been quoted in Table 1. These second possible date ranges are statistically far less likely than the Anglo-Saxon dates and can be excluded on archaeological grounds (P. Buzby pers. comm.), thus they are not depicted in Figure 5.

Figure 5 also shows that the date ranges inferred for features, 1WB, 3WB and 4WB are broad, covering more than 200 years, despite their mean TRM directions, quoted in Table 1, being determined with relatively good precision. There are two reasons for this:

i) The precision with which declination can be determined varies inversely with the cosine of inclination, owing to the way that inclination and declination are defined in terms of projection onto a sphere. Hence, the precision with which declination can be determined is lower when, as in the Anglo-Saxon period, the inclination of the Earth's magnetic field in the UK was steep. As much of the movement of the pole during the Anglo-Saxon period was change in declination rather than inclination, the precision with which features last fired in this period can be dated is relatively poor.

ii) The virtual geomagnetic pole position observed from the UK was relatively invariant between about 550 AD and 800 AD. This is represented on the UK Archaeomagnetic Calibration Curve by a tight loop (see, for instance, Figure 9). The precision with which features can be dated archaeomagnetically is proportional to the speed at which the geomagnetic pole was moving when they were last fired and is much reduced during such slow moving periods.

Given the considerable degree of overlap between the date ranges of features 1WB, 3WB and 4WB, it is interesting to consider whether their dates of last firing might be contemporary. This question is of particular relevance given the archaeological relationships between the three. Feature 1WB appeared to be a resurfacing of 3WB and might thus be expected to date from later. Feature 4WB was the burnt natural soil within the kerbed area associated with 1WB/3WB and so may have acquired it TRM at the same time as one of the two firing events dated by them.

Comparing the mean TRM directions of 1WB and 3WB using the test of McFadden and Lowes (1981) indicates a probability of only 1.6% that these two mean TRM directions are both estimates of the same true direction. Hence, the hypothesis that 1WB and 3WB both acquired their TRM at the same time may be rejected at the 5% level. So the firing of surface 3WB is likely to have significantly predated that of 1WB which overlay it. However, given the poor precision of the date range inferred for 3WB it is only possible to say that this firing occurred some time after 560 AD and before the firing of 1WB.

Using the same test to compare the mean TRM directions of 1WB with 4WB yields a probability of 79.9% that the two are estimates of the same true direction. Although this probability is not high enough to accept the hypothesis that both were fired at the same time at the 95% confidence level, there is still only about one chance in five that they date different firing events. Contemporary dates for the two might be expected on archaeological grounds if fires were lit on feature 1WB/3WB and used to heat the whole area within the stone kerb to a considerable temperature. In this case, each time a fire was lit, the surrounding soil floor (4WB) would be reheated and a new TRM would overprint that acquired previously. The final TRM acquired by 4WB would thus be associated with the last firing of 1WB/3WB and this would also be dated by the TRM in the uppermost layer of the surface on which the heating fire was set (1WB).

On this basis, all the samples used to calculate the mean TRM direction of 4WB were combined with the samples from 1WB to calculate a joint mean. This is quoted in Table 1 and depicted in Figure 5 as 1+4WB. Given the assumption that the mean TRMs in features 1WB and 4WB both date the same firing event, a tighter date range for the last firing of the drier can be determined, and it most probably occurred between 730 and 790 AD (63% confidence level).

Finally, it is interesting to note that the date for the last firing of feature 2WB is some 250 years later than the dates inferred for the three other features. This suggests a considerable time span between these events on the site.

P. Linford
Archaeometry Branch,
Centre for Archaeology, English Heritage.

Date of report: 23/11/2001

Archaeomagnetic Date Summary

Archaeomagnetic ID:	**1WB**
Feature:	**context 30980**
Location:	**Longitude 0.6°W, Latitude 54.5°N**
Number of Samples (taken/used in mean):	**18/18**
AF Demagnetisation Applied:	**10mT**
Distortion Correction Applied:	**+2.4°**
Declination (at Meriden):	**6.9° (6.8°)**
Inclination (at Meriden):	**77.2° (75.9°)**
Alpha-95:	**1.8°**
k:	**390.3**
Date range (63% confidence):	**685 AD to 795 AD**
Date range (95% confidence):	**560 AD to 810 AD**

Archaeomagnetic ID:	**2WB**
Feature:	**context 30985**
Location:	**Longitude 0.6°W, Latitude 54.5°N**
Number of Samples (taken/used in mean):	**13/7**
AF Demagnetisation Applied:	**5mT**
Distortion Correction Applied:	**+2.4°**
Declination (at Meriden):	**30.4° (28.9°)**
Inclination (at Meriden):	**69.6° (68.1°)**
Alpha-95:	**3.6°**
k:	**277.6**
Date range (63% confidence):	**980 AD to 1045 AD**
Date range (95% confidence):	**920 AD to 1085 AD or 600 BC to 400 BC**

Archaeomagnetic ID:	**3WB**
Feature:	**context 39201**
Location:	**Longitude 0.6°W, Latitude 54.5°N**
Number of Samples (taken/used in mean):	**14/10**
AF Demagnetisation Applied:	**5mT**
Distortion Correction Applied:	**+2.4°**
Declination (at Meriden):	**22.9° (21.7°)**
Inclination (at Meriden):	**75.6° (74.3°)**
Alpha-95:	**3.1°**
k:	**246.0**
Date range (63% confidence):	**undatable**
Date range (95% confidence):	**560 AD to 850 AD or 535 BC to 200 BC**

Archaeomagnetic ID:	**4WB**
Feature:	**context 39211**
Location:	**Longitude 0.6^{o}W, Latitude 54.5^{o}N**
Number of Samples (taken/used in mean):	**14/13**
AF Demagnetisation Applied:	**5mT**
Distortion Correction Applied:	**+2.4^{o}**
Declination (at Meriden):	**6.8^{o} (6.7^{o})**
Inclination (at Meriden):	**76.3^{o} (75.1^{o})**
Alpha-95:	**2.5^{o}**
k:	**268.0**
Date range (63% confidence):	**615 AD to 800 AD**
Date range (95% confidence):	**560 AD to 825 AD**

	NRM Measurements				After Partial Demagnetisation			
Sample	Material	Dec°	Inc°	J(mAm^{-1})	AF(mT)	Dec°	Inc°	J(mAm^{-1})	R
1WB01	Clay	17.4	80.5	10130.7	10.0	26.0	80.9	9371.8	
1WB02	Clay	-6.4	78.9	16453.0	10.0	-8.7	79.6	13458.0	
1WB03	Clay	3.0	76.6	6770.2	10.0	6.9	76.7	6076.4	
1WB04	Clay	-1.5	75.5	7420.6	10.0	-4.7	75.6	6625.5	
1WB05	Clay	4.4	78.3	19893.4	10.0	2.4	77.3	16727.4	
1WB06	Clay	17.2	76.1	9618.1	10.0	22.8	76.8	7588.2	
1WB07	Clay	18.0	76.9	16630.9	10.0	19.3	77.8	13504.4	
1WB08	Clay	10.9	75.9	14567.7	10.0	13.8	76.1	11744.4	
1WB09	Clay	-8.8	73.6	20186.7	10.0	-2.4	75.7	16060.8	
1WB10	Clay	7.3	76.4	23227.3	10.0	11.6	76.8	18578.6	
1WB11	Clay	-1.3	71.6	9423.3	10.0	0.6	71.1	6394.5	
1WB12	Clay	6.8	76.3	38706.0	10.0	8.2	76.3	29511.4	
1WB13	Clay	2.3	72.4	32543.6	10.0	4.2	73.1	23044.5	
1WB14	Clay	3.2	69.9	13359.3	10.0	8.5	70.8	10663.4	
1WB15	Clay	1.4	71.1	14347.2	10.0	0.6	71.2	10433.0	
1WB16	Clay	5.5	69.2	17966.1	10.0	9.6	70.8	11247.9	
1WB17	Clay	5.7	69.0	8981.4	10.0	5.9	69.0	5545.5	
1WB18	Clay	10.7	68.8	13507.7	10.0	9.4	68.1	9004.8	

Table 2: NRM measurements of samples and measurements after partial AF demagnetisation for feature 1WB. J = magnitude of magnetisation vector; AF = peak alternating field strength of demagnetising field; R = sample rejected from mean calculation.

	1WB05			1WB16		
AF(mT)	Dec°	Inc°	J(mAm^{-1})	Dec°	Inc°	J(mAm^{-1})
0.0	6.6	77.9	20119.3	9.4	70.5	17891.5
2.5	1.0	77.3	19952.9	8.4	70.3	17506.1
5.0	1.8	77.2	19354.5	8.6	70.7	16198.1
10.0	2.4	77.3	16727.4	9.6	70.8	11247.9
15.0	4.6	77.0	11773.7	9.6	71.1	5496.2
20.0	6.5	76.8	7677.8	9.9	71.7	2442.9
30.0	11.2	76.0	3826.2	5.7	69.9	975.0
50.0	10.5	74.7	1806.5	20.7	75.3	493.4
75.0	11.4	73.8	762.2	-	-	-
100.0	-37.6	71.7	336.8	-	-	-

Table 3: Incremental partial demagnetisation measurements for samples 1WB05 and 1WB16.

	NRM Measurements				After Partial Demagnetisation			
Sample	Material	Dec°	Inc°	J(mAm^{-1})	AF(mT)	Dec°	Inc°	J(mAm^{-1})	R
2WB01	Clay	4.6	63.3	648.7	-	-	-	-	R
2WB02	Clay	87.1	4.8	1163.1	-	-	-	-	R
2WB03	Clay	37.1	78.7	399.1	-	-	-	-	R
2WB04	Clay	106.3	62.6	698.2	-	-	-	-	R
2WB05	Clay	69.1	68.7	357.8	-	-	-	-	R
2WB06	S'stone	29.6	66.7	10.1	5.0	32.5	64.8	4.7	
2WB07	S'stone	37.6	72.2	12.2	5.0	26.8	66.2	6.5	
2WB08	S'stone	19.6	74.3	22.9	5.0	11.1	69.0	12.2	
2WB09	S'stone	31.8	69.8	14.2	5.0	40.7	67.6	9.0	
2WB10	S'stone	72.5	65.3	609.9	5.0	74.1	64.1	549.9	R
2WB11	S'stone	33.3	72.1	38.8	5.0	32.5	71.5	32.0	
2WB12	S'stone	28.3	70.4	13.5	5.0	26.7	68.9	7.7	
2WB13	S'stone	35.4	69.2	11.6	5.0	38.5	60.7	6.7	

Table 4: NRM measurements of samples and measurements after partial AF demagnetisation for feature 2WB. J = magnitude of magnetisation vector; AF = peak alternating field strength of demagnetising field; R = sample rejected from mean calculation; S'stone = sandstone.

	2WB09			2WB10		
AF(mT)	Dec°	Inc°	J(mAm^{-1})	Dec°	Inc°	J(mAm^{-1})
0.0	37.3	66.1	13.0	73.0	64.2	613.5
1.0	36.1	67.7	11.2	-	-	-
2.5	33.8	66.5	9.9	73.5	64.3	590.7
5.0	40.7	67.6	9.0	74.1	64.1	549.9
10.0	40.7	64.3	6.7	74.5	63.6	371.4
15.0	42.1	68.1	5.9	74.6	63.2	198.1
20.0	37.6	67.6	4.6	73.6	63.4	119.6
30.0	41.9	65.1	3.5	68.8	63.8	70.9
50.0	30.0	62.3	2.5	71.0	67.6	47.3
75.0	49.0	66.0	1.8	-	-	-

Table 5: Incremental partial demagnetisation measurements for samples 2WB09 and 2WB10.

	NRM Measurements				After Partial Demagnetisation			
Sample	Material	Dec°	Inc°	J(mAm^{-1})	AF(mT)	Dec°	Inc°	J(mAm^{-1})	R
3WB01	Clay	17.3	67.9	2616.3	5.0	18.9	67.0	2401.9	
3WB02	Clay	53.7	79.4	6034.7	5.0	53.0	79.8	5359.3	R
3WB03	Clay	45.1	77.1	2351.9	5.0	47.7	76.9	2034.2	
3WB04	Clay	-21.7	85.4	15389.8	5.0	-21.7	85.4	14919.8	R
3WB05	Clay	-34.0	81.3	15733.5	5.0	-35.5	82.1	14546.3	R
3WB06	Clay	6.9	72.4	4437.1	5.0	7.2	73.2	3844.1	
3WB07	Clay	73.3	80.0	15555.8	5.0	75.8	80.2	13927.2	R
3WB08	Clay	30.0	77.2	20390.6	5.0	28.8	76.4	18057.3	
3WB09	Clay	45.3	72.2	10567.5	5.0	44.3	72.0	8922.2	
3WB10	Clay	-3.0	77.2	10262.7	5.0	-4.7	77.1	5374.0	
3WB11	Clay	21.8	71.2	3993.9	5.0	13.1	70.5	2409.9	
3WB12	Clay	23.0	73.1	11421.5	5.0	28.3	73.1	9316.1	
3WB13	Clay	29.9	71.9	15994.5	5.0	34.6	73.0	13538.2	
3WB14	Clay	15.4	69.3	5832.5	5.0	15.0	68.6	5050.0	

Table 6: NRM measurements of samples and measurements after partial AF demagnetisation for feature 3WB. J = magnitude of magnetisation vector; AF = peak alternating field strength of demagnetising field; R = sample rejected from mean calculation.

	3WB02			3WB05		
AF(mT)	Dec°	Inc°	J(mAm^{-1})	Dec°	Inc°	J(mAm^{-1})
0.0	53.6	79.6	6047.4	-35.2	81.5	16328.4
2.5	53.3	79.8	5892.2	-35.7	82.0	15886.5
5.0	53.0	79.8	5359.3	-35.5	82.1	14546.3
10.0	51.2	79.2	2996.2	-36.3	82.0	8868.3
15.0	45.6	78.2	1034.9	-36.4	81.7	4960.5
20.0	42.2	76.8	463.1	-37.8	81.4	3552.0
30.0	33.7	76.1	208.6	-35.3	80.9	2622.3
50.0	-	-	-	-39.3	79.7	2222.7
75.0	-	-	-	-40.8	80.3	2035.5

Table 7: Incremental partial demagnetisation measurements for samples 3WB02 and 3WB05.

	3WB10			3WB13		
AF(mT)	Dec°	Inc°	J(mAm^{-1})	Dec°	Inc°	J(mAm^{-1})
0.0	-6.4	77.1	10140.2	33.4	72.6	15197.1
2.5	-6.3	77.3	8487.6	34.4	73.1	14666.5
5.0	-4.7	77.1	5374.0	34.6	73.0	13538.2
7.5	-5.2	76.2	2761.8	-	-	-
10.0	-5.2	74.5	1538.1	35.3	73.1	9165.3
15.0	-8.5	78.4	907.6	35.4	73.5	5132.7
20.0	-4.7	74.1	676.4	33.0	73.9	2666.8
30.0	2.6	65.6	461.0	31.5	72.0	1054.5
50.0	-	-	-	19.1	73.7	526.5
75.0	-	-	-	22.8	69.4	378.9

Table 8: Incremental partial demagnetisation measurements for samples 3WB10 and 3WB13.

	NRM Measurements				After Partial Demagnetisation			
Sample	Material	Dec°	Inc°	J(mAm^{-1})	AF(mT)	Dec°	Inc°	J(mAm^{-1})	R
4WB01	Clay	-7.9	76.8	1425.7	5.0	-10.8	75.9	1067.2	
4WB02	Clay	-8.1	77.8	2679.3	5.0	-1.7	77.5	1853.0	
4WB03	Clay	1.7	70.8	708.7	5.0	5.2	69.4	548.5	
4WB04	Clay	13.8	72.3	4271.0	5.0	20.5	72.4	3292.1	
4WB05	Clay	0.4	75.0	4188.5	5.0	1.7	73.9	3592.0	
4WB06	Clay	-5.7	79.8	3071.8	5.0	2.6	80.3	2547.6	
4WB07	Clay	-17.2	76.4	2653.6	5.0	-16.0	75.8	2460.8	
4WB08	Clay	6.9	78.6	3702.2	5.0	14.9	76.7	2912.4	
4WB09	Clay	-5.7	77.4	781.1	5.0	-4.6	77.3	645.7	
4WB10	Clay	16.6	68.8	957.2	5.0	16.7	68.4	693.0	
4WB11	Clay	-8.0	62.7	10475.0	5.0	-8.0	63.1	9115.7	R
4WB12	Clay	20.3	75.0	1994.4	5.0	20.0	73.5	1630.3	
4WB13	Clay	14.7	73.1	205.2	5.0	14.9	71.7	163.4	
4WB14	Clay	8.3	66.4	885.2	5.0	7.0	65.6	679.7	

Table 9: NRM measurements of samples and measurements after partial AF demagnetisation for feature 4WB. J = magnitude of magnetisation vector; AF = peak alternating field strength of demagnetising field; R = sample rejected from mean calculation.

	4WB02			4WB08			4WB11		
AF(mT)	Dec°	Inc°	J(mAm^{-1})	Dec°	Inc°	J(mAm^{-1})	Dec°	Inc°	J(mAm^{-1})
0.0	-0.9	78.9	2654.7	8.7	78.2	3654.0	-6.6	63.5	10368.6
2.5	-2.1	77.7	2401.1	13.0	77.2	3359.6	-7.5	63.5	10023.7
5.0	-1.7	77.5	1853.0	14.9	76.7	2912.4	-8.0	63.1	9115.7
10.0	-12.1	79.0	679.6	15.8	76.2	1599.2	-7.6	62.7	5813.6
15.0	-60.3	79.4	191.3	14.0	75.4	612.4	-8.8	61.5	2654.5
20.0	-105.5	66.1	89.9	10.9	73.9	275.2	-9.0	62.3	1112.9
30.0	-97.8	54.2	46.9	-11.8	82.5	119.1	18.8	70.1	254.5

Table 10: Incremental partial demagnetisation measurements for samples 4WB02, 4WB08 and 4WB11.

Appendix: Standard Procedures for Sampling and Measurement

1) Sampling

One of three sampling techniques is employed depending on the consistency of the material (Clark, Tarling and Noel 1988):

a) **Consolidated materials:** Rock and fired clay samples are collected by the disc method. Several small levelled plastic discs are glued to the feature, marked with an orientation line related to True North, then removed with a small piece of the material attached.

b) **Unconsolidated materials:** Sediments are collected by the tube method. Small pillars of the material are carved out from a prepared platform, then encapsulated in levelled plastic tubes using plaster of Paris. The orientation line is then marked on top of the plaster.

c) **Plastic materials:** Waterlogged clays and muds are sampled in a similar manner to method 1b) above; however, the levelled plastic tubes are pressed directly into the material to be sampled.

2) Physical Analysis

a) Magnetic remanences are measured using a slow speed spinner fluxgate magnetometer (Molyneux et al. 1972; see also Tarling 1983, p84; Thompson and Oldfield 1986, p52).

b) Partial demagnetisation is achieved using the alternating magnetic field method (As 1967; Creer 1959; see also Tarling 1983, p91; Thompson and Oldfield 1986, p59), to remove viscous magnetic components if necessary. Demagnetising fields are measured in milli-Tesla (mT), figures quoted being for the peak value of the field.

3) Remanent Field Direction

a) The remanent field direction of a sample is expressed as two angles, declination (Dec) and inclination (Inc), both quoted in degrees. Declination represents the bearing of the field relative to true north, angles to the east being positive; inclination represents the angle of dip of this field.

b) Aitken and Hawley (1971) have shown that the angle of inclination in measured samples is likely to be distorted owing to magnetic refraction. The phenomenon is not well understood but is known to depend on the position the samples occupied within the structure. The corrections recommended by Aitken and Hawley are applied, where appropriate, to measured inclinations, in keeping with the practise of Clark, Tarling and Noel (1988).

c) Individual remanent field directions are combined to produce the mean remanent field direction using the statistical method developed by R. A. Fisher (1953). The quantity α_{95}, "alpha-95", is quoted with mean field directions and is a measure of the precision of the determination (see Aitken 1990, p247). It is analogous to the standard error statistic for scalar quantities; hence the smaller its value, the better the precision of the date.

d) For the purposes of comparison with standardised UK calibration data, remanent field directions are adjusted to the values they would have had if the feature had been located at Meriden, a standard reference point. The adjustment is done using the method suggested by Noel (Tarling 1983, p116).

4) Calibration

a) Material less than 3000 years old is dated using the archaeomagnetic calibration curve compiled by Clark, Tarling and Noel (1988).

b) Older material is dated using the lake sediment data compiled by Turner and Thompson (1982).

c) Dates are normally given at the 63% and 95% confidence levels. However, the quality of the measurement and the estimated reliability of the calibration curve for the period in question are not taken into account, so this figure is only approximate. Owing to crossovers and contiguities in the curve, alternative dates are sometimes given. It may be possible to select the correct alternative using independent dating evidence.

d) As the thermoremanent effect is reset at each heating, all dates for fired material refer to the final heating.

e) Dates are prefixed by "cal", for consistency with the new convention for calibrated radiocarbon dates (Mook 1986).

References

Aitken, M. J. 1990. *Science-based Dating in Archaeology*. London: Longman.

Aitken, M. J. and H. N. Hawley 1971. Archaeomagnetism: evidence for magnetic refraction in kiln structures. *Archaeometry* **13**, 83-85.

As, J. A. 1967. The a.c. demagnetisation technique, in *Methods in Palaeomagnetism*, D. W. Collinson, K. M. Creer and S. K. Runcorn (eds). Amsterdam: Elsevier.

Clark, A. J., D. H. Tarling and M. Noel 1988. Developments in Archaeomagnetic Dating in Britain. *J. Arch. Sci.* **15**, 645-667.

Creer, K. M. 1959. A.C. demagnetisation of unstable Triassic Keuper Marls from S. W. England. *Geophys. J. R. Astr. Soc.* **2**, 261-275.

Fisher, R. A. 1953. Dispersion on a sphere. *Proc. R. Soc. London A* **217**, 295-305.

McFadden, P. L. and Lowes, F. J. 1981. The discrimination of mean directions drawn from Fisher distributions. *Geophys. J. R. Astr. Soc.* **67**, 19-33.

Molyneux, L., R. Thompson, F. Oldfield and M. E. McCallan 1972. Rapid measurement of the remanent magnetisation of long cores of sediment. *Nature* **237**, 42-43.

Mook, W. G. 1986. Recommendations/Resolutions Adopted by the Twelfth International Radiocarbon Conference. *Radiocarbon* **28**, M. Stuiver and S. Kra (eds), 799.

Tarling, D. H. 1983. *Palaeomagnetism*. London: Chapman and Hall.

Thompson, R. and F. Oldfield 1986. *Environmental Magnetism*. London: Allen and Unwin.

Turner, G. M. and R. Thompson 1982. Detransformation of the British geomagnetic secular variation record for Holocene times. *Geophys. J. R. Astr. Soc.* **70**, 789-792.

a)

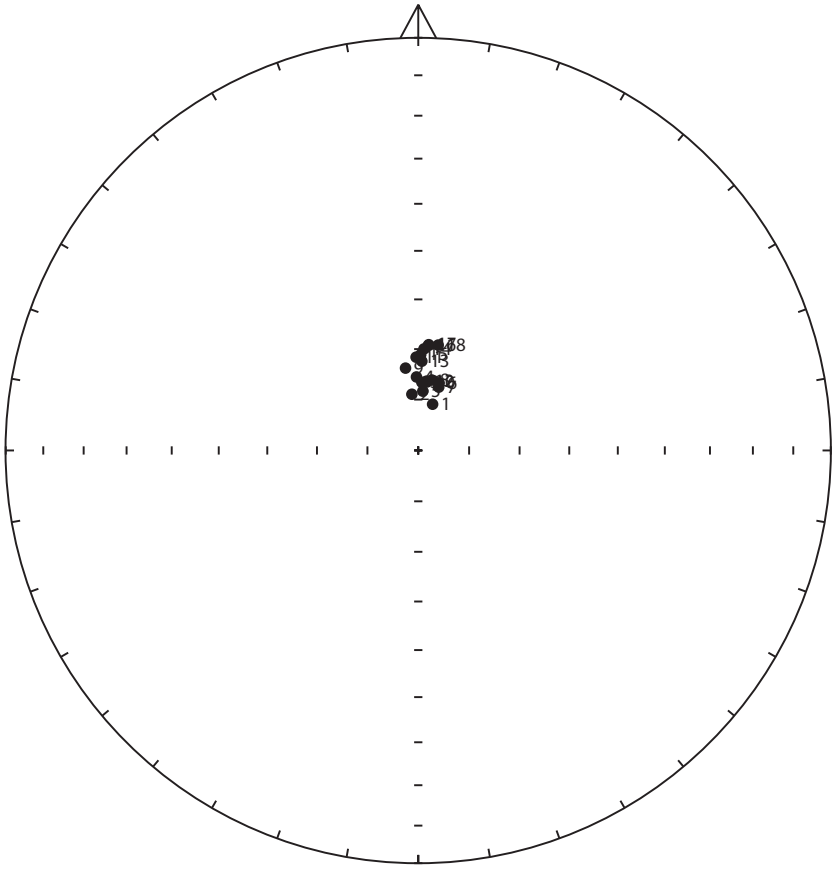

b)

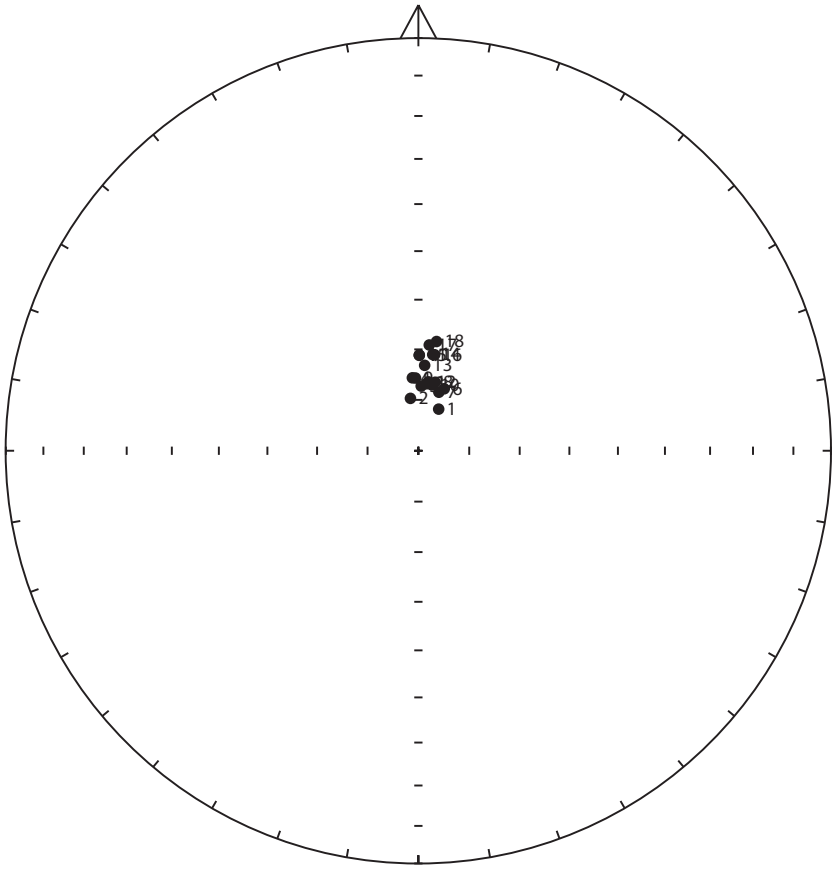

Figure 6: a) Distribution of NRM directions of samples from feature 1WB represented as an equal area stereogram. In this projection declination increases clockwise with zero being at 12 o'clock while inclination increases from zero at the equator to 90 degrees in the centre of the projection. Open circles represent negative inclinations. b) Distribution of thermoremanent directions of magnetisation of the same samples after partial AF demagnetisation to 10mT.

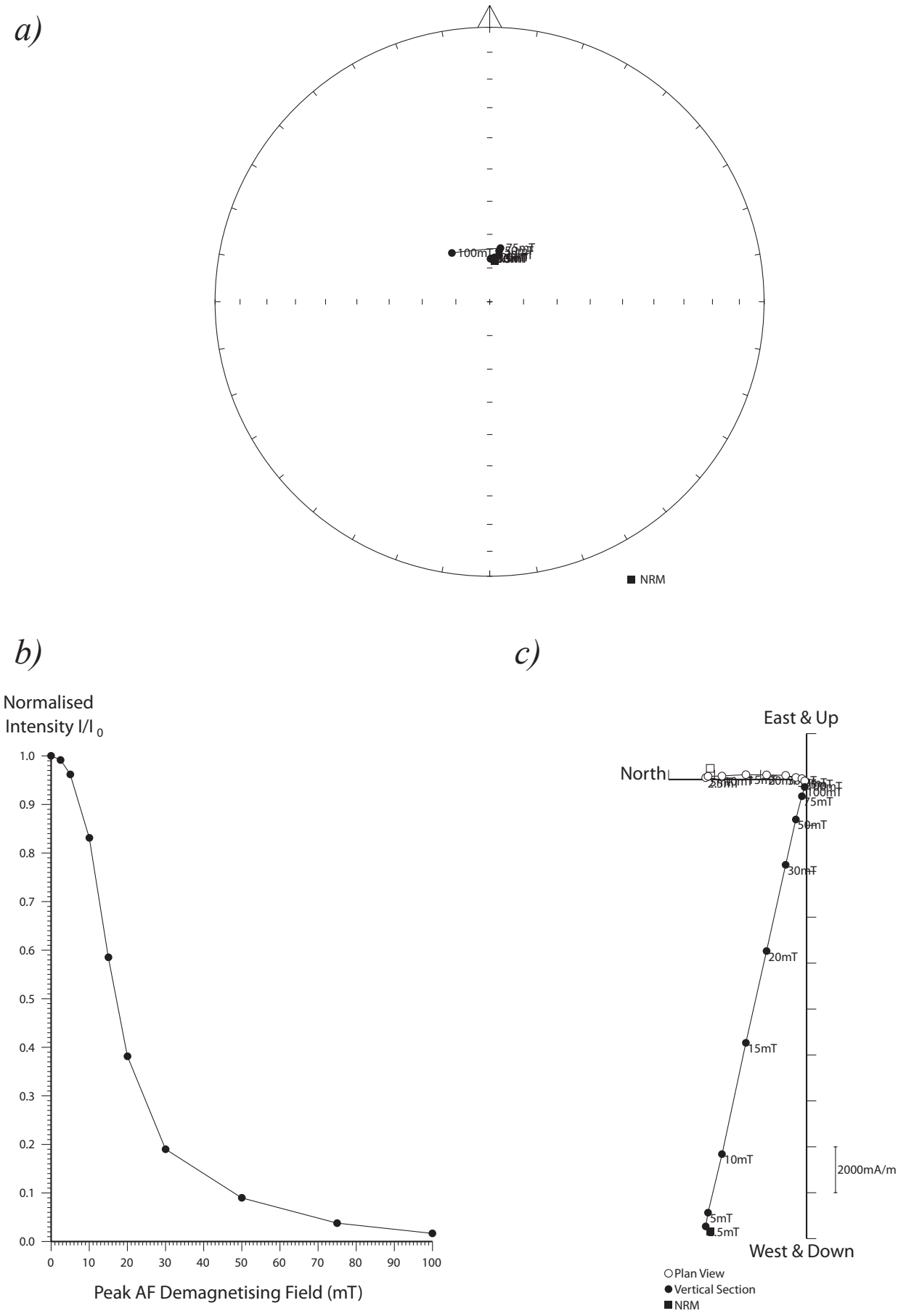

Figure 7: Stepwise AF demagnetisation of sample 1WB05. Diagram a) depicts the variation of the remanent direction as an equal area stereogram (declination increases clockwise, while inclination increases from zero at the equator to 90 degrees at the centre of the projection); b) shows the normalised change in remanence intensity as a function of the demagnetising field; c) shows the changes in both direction and intensity as a vector endpoint projection.

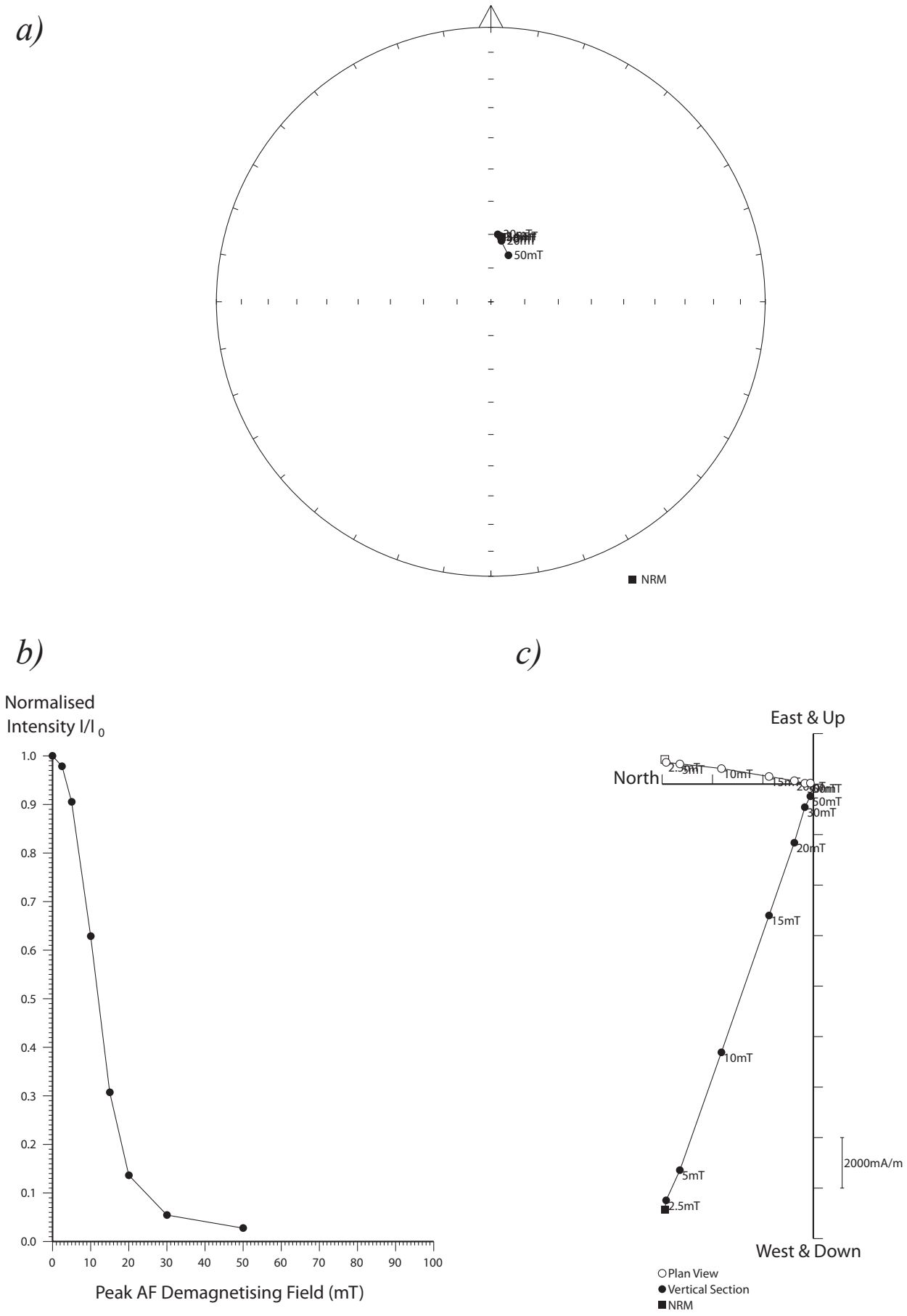

Figure 8: Stepwise AF demagnetisation of sample 1WB16. Diagram a) depicts the variation of the remanent direction as an equal area stereogram (declination increases clockwise, while inclination increases from zero at the equator to 90 degrees at the centre of the projection); b) shows the normalised change in remanence intensity as a function of the demagnetising field; c) shows the changes in both direction and intensity as a vector endpoint projection.

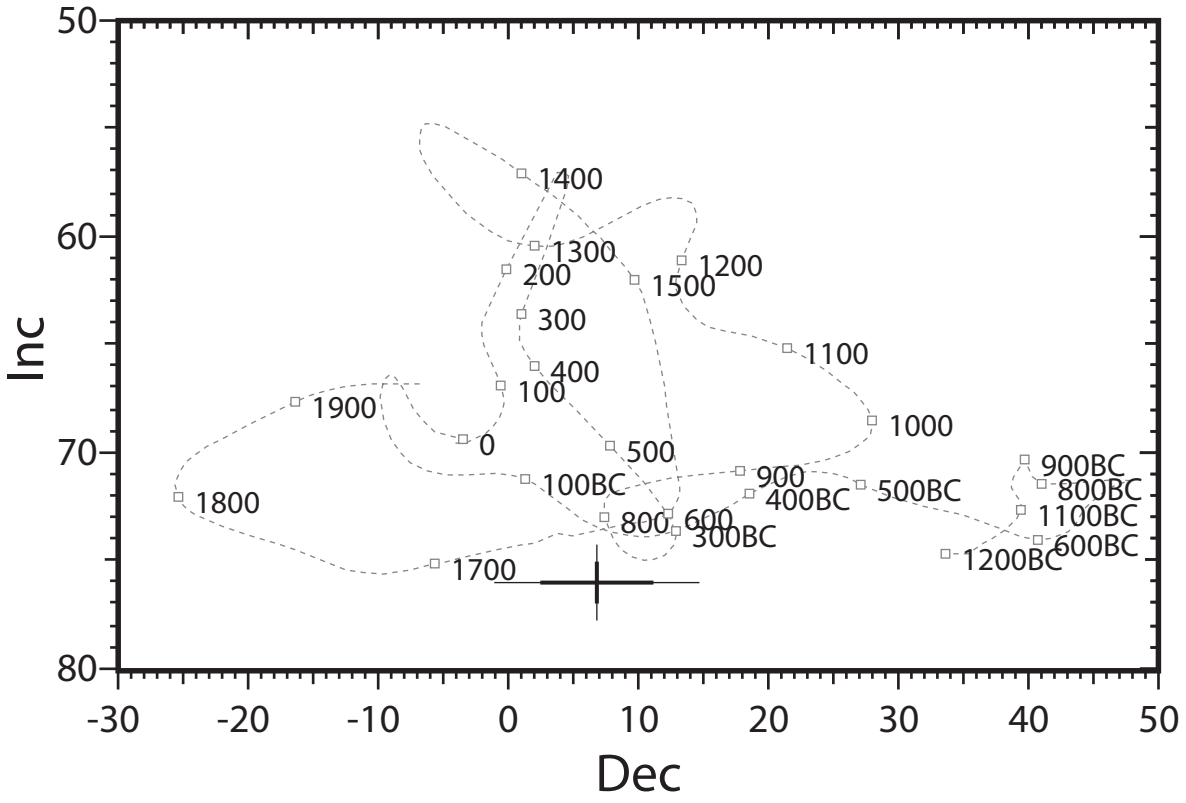

Figure 9: Comparison of the mean thermoremanent vector of samples from feature 1WB after 10mT partial AF demagnetisation with the UK master calibration curve. Thick error bar lines represent 63% confidence limits and narrow lines 95% confidence limits.

a)

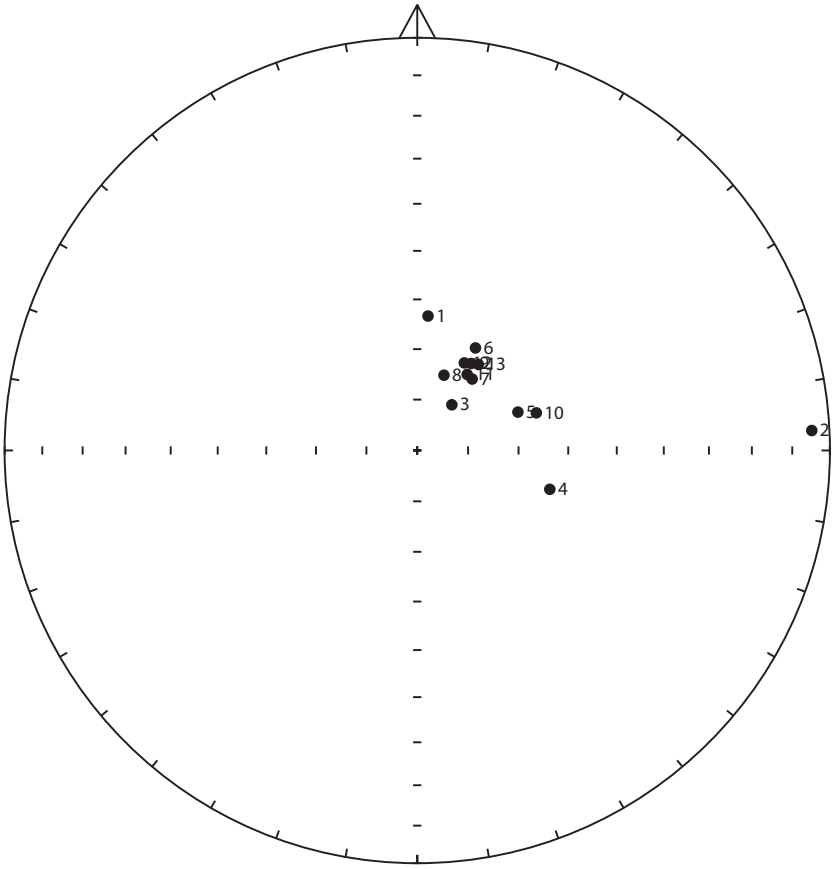

b)

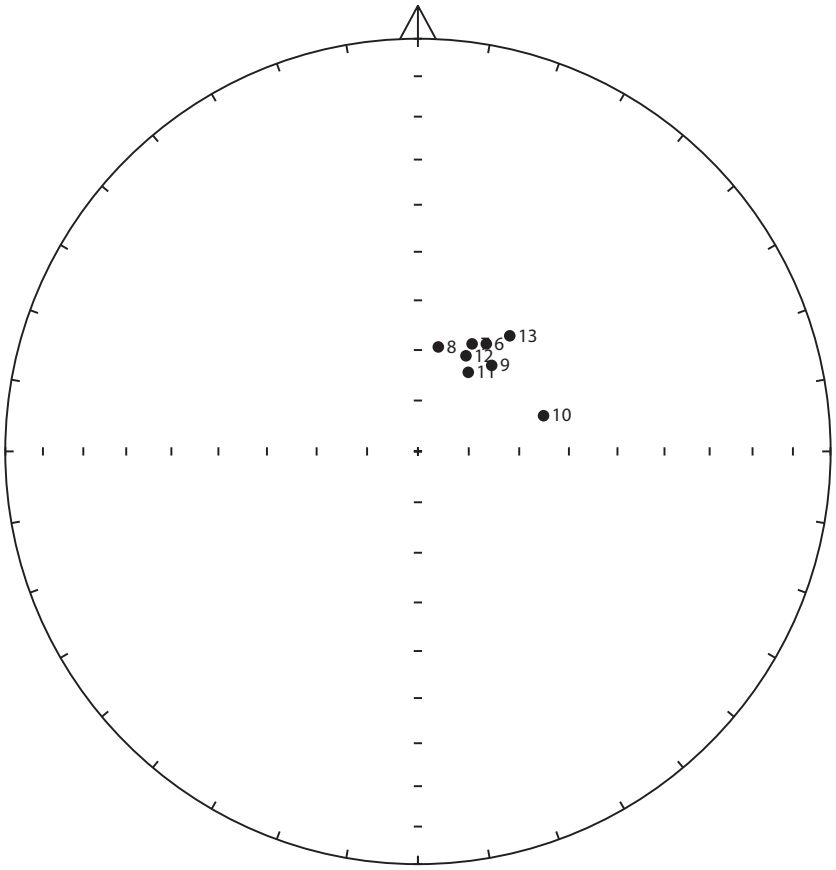

Figure 10: a) Distribution of NRM directions of samples from feature 2WB represented as an equal area stereogram. In this projection declination increases clockwise with zero being at 12 o'clock while inclination increases from zero at the equator to 90 degrees in the centre of the projection. Open circles represent negative inclinations. b) Distribution of thermoremanent directions of magnetisation of the same samples after partial AF demagnetisation to 5mT.

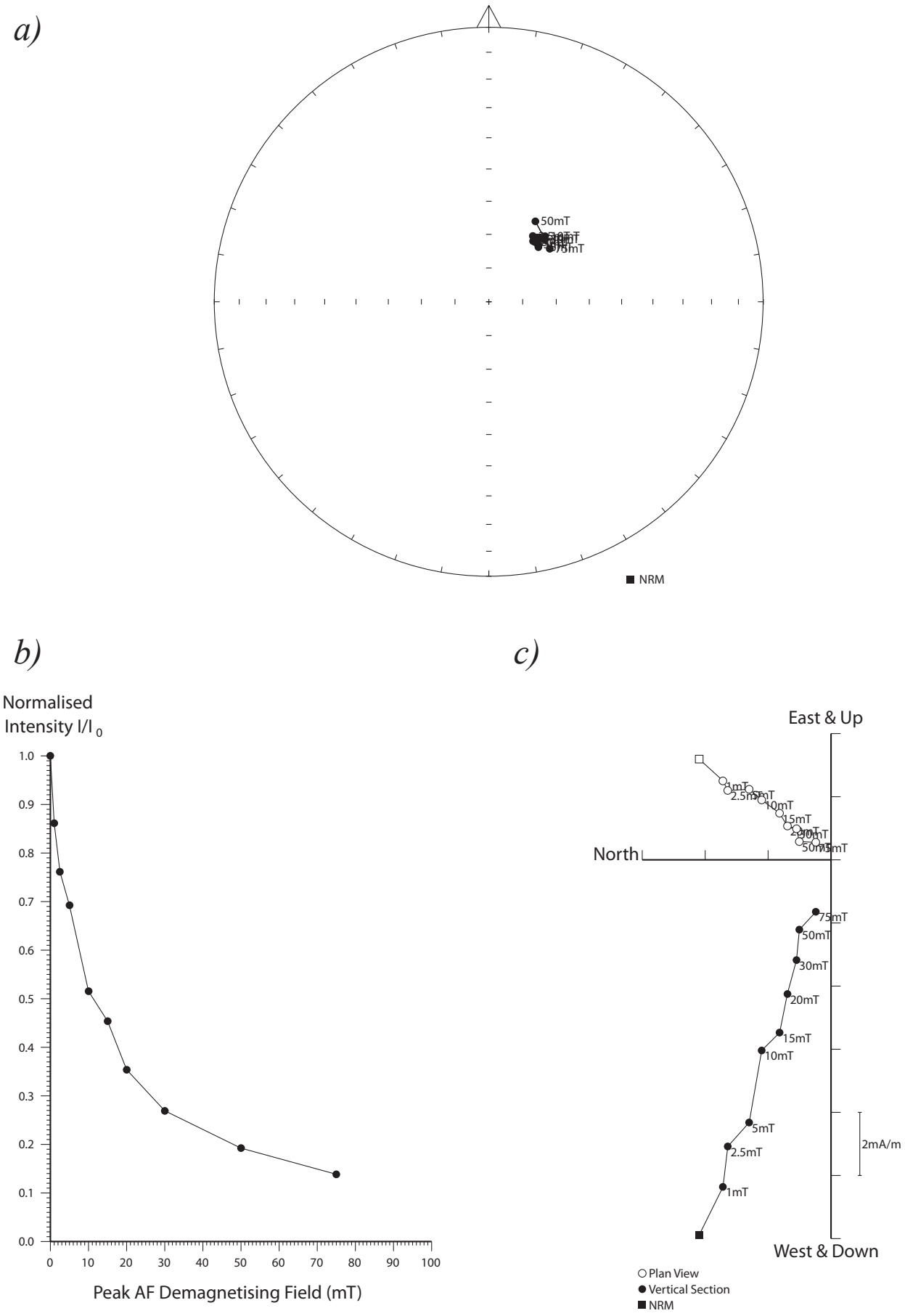

Figure 11: Stepwise AF demagnetisation of sample 2WB09. Diagram a) depicts the variation of the remanent direction as an equal area stereogram (declination increases clockwise, while inclination increases from zero at the equator to 90 degrees at the centre of the projection); b) shows the normalised change in remanence intensity as a function of the demagnetising field; c) shows the changes in both direction and intensity as a vector endpoint projection.

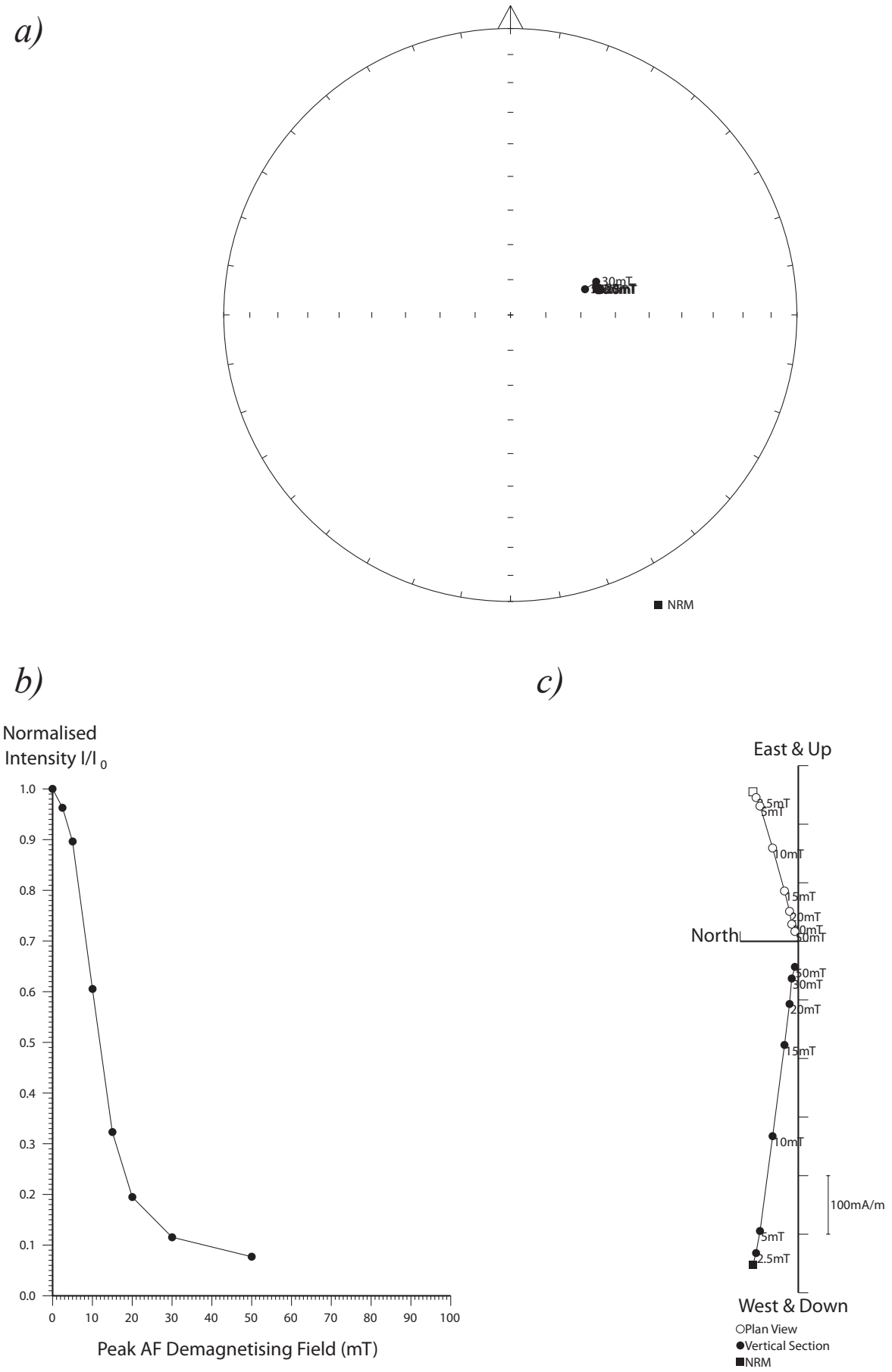

Figure 12: Stepwise AF demagnetisation of sample 2WB10. Diagram a) depicts the variation of the remanent direction as an equal area stereogram (declination increases clockwise, while inclination increases from zero at the equator to 90 degrees at the centre of the projection); b) shows the normalised change in remanence intensity as a function of the demagnetising field; c) shows the changes in both direction and intensity as a vector endpoint projection.

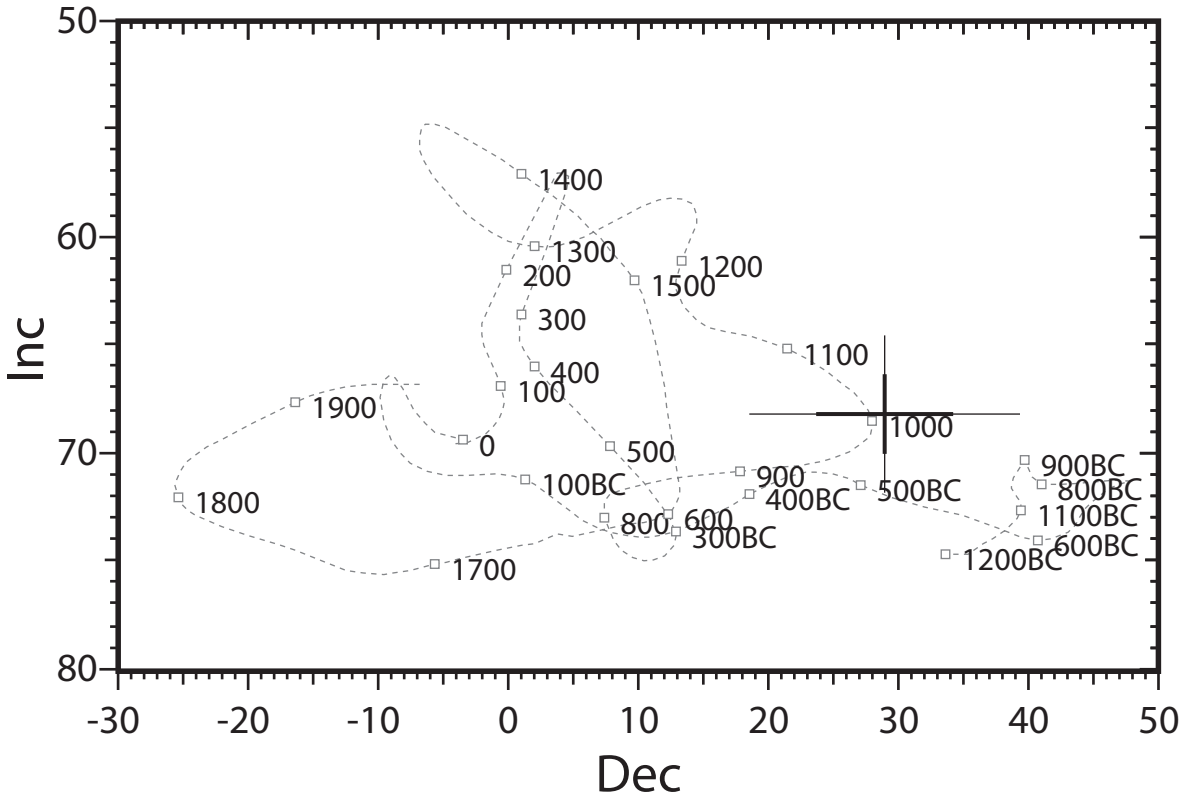

Figure 13: Comparison of the mean thermoremanent vector of samples 2wb06-09, 2WB11-13 from feature 2WB after 5mT partial AF demagnetisation with the UK master calibration curve. Thick error bar lines represent 63% confidence limits and narrow lines 95% confidence limits.

a)

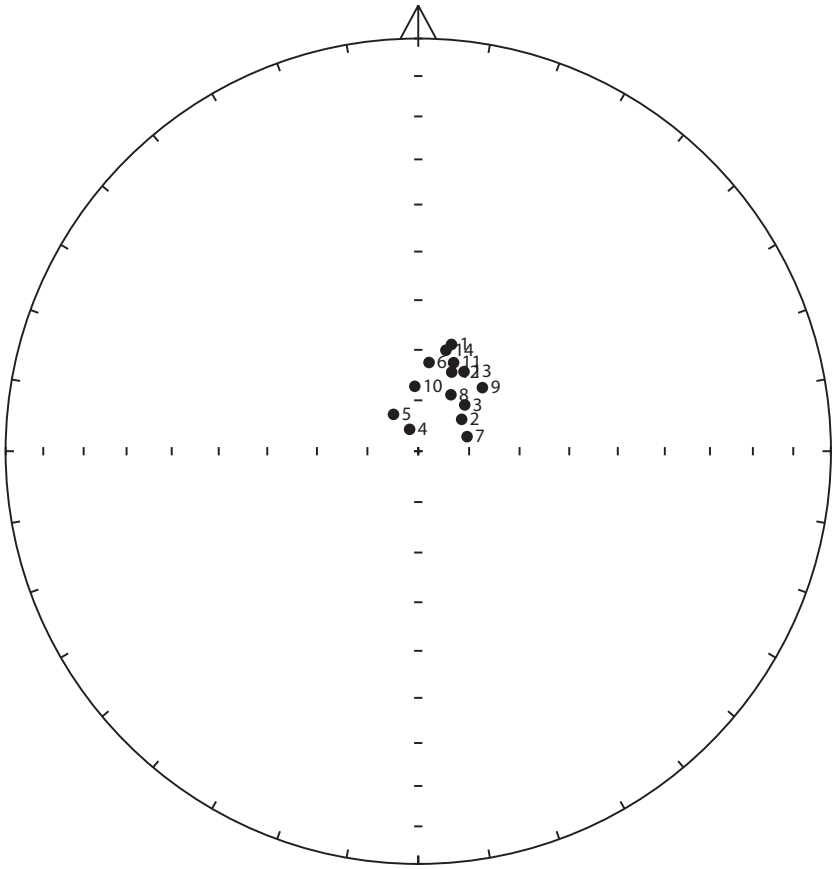

b)

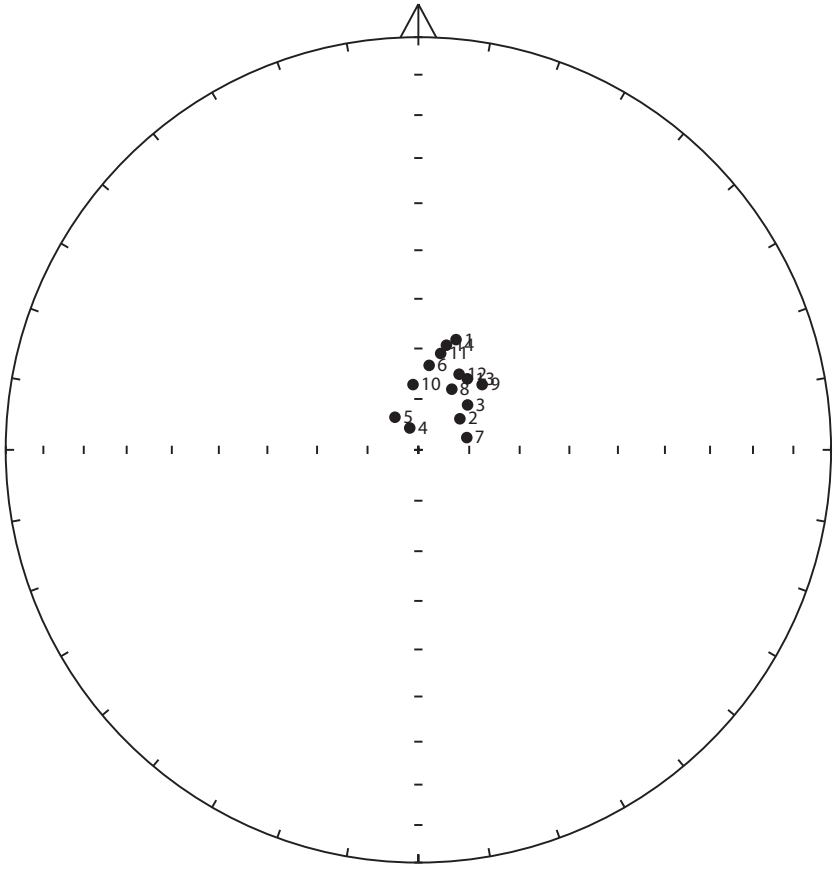

Figure 14: a) Distribution of NRM directions of samples from feature 3WB represented as an equal area stereogram. In this projection declination increases clockwise with zero being at 12 o'clock while inclination increases from zero at the equator to 90 degrees in the centre of the projection. Open circles represent negative inclinations. b) Distribution of thermoremanent directions of magnetisation of the same samples after partial AF demagnetisation to 5mT.

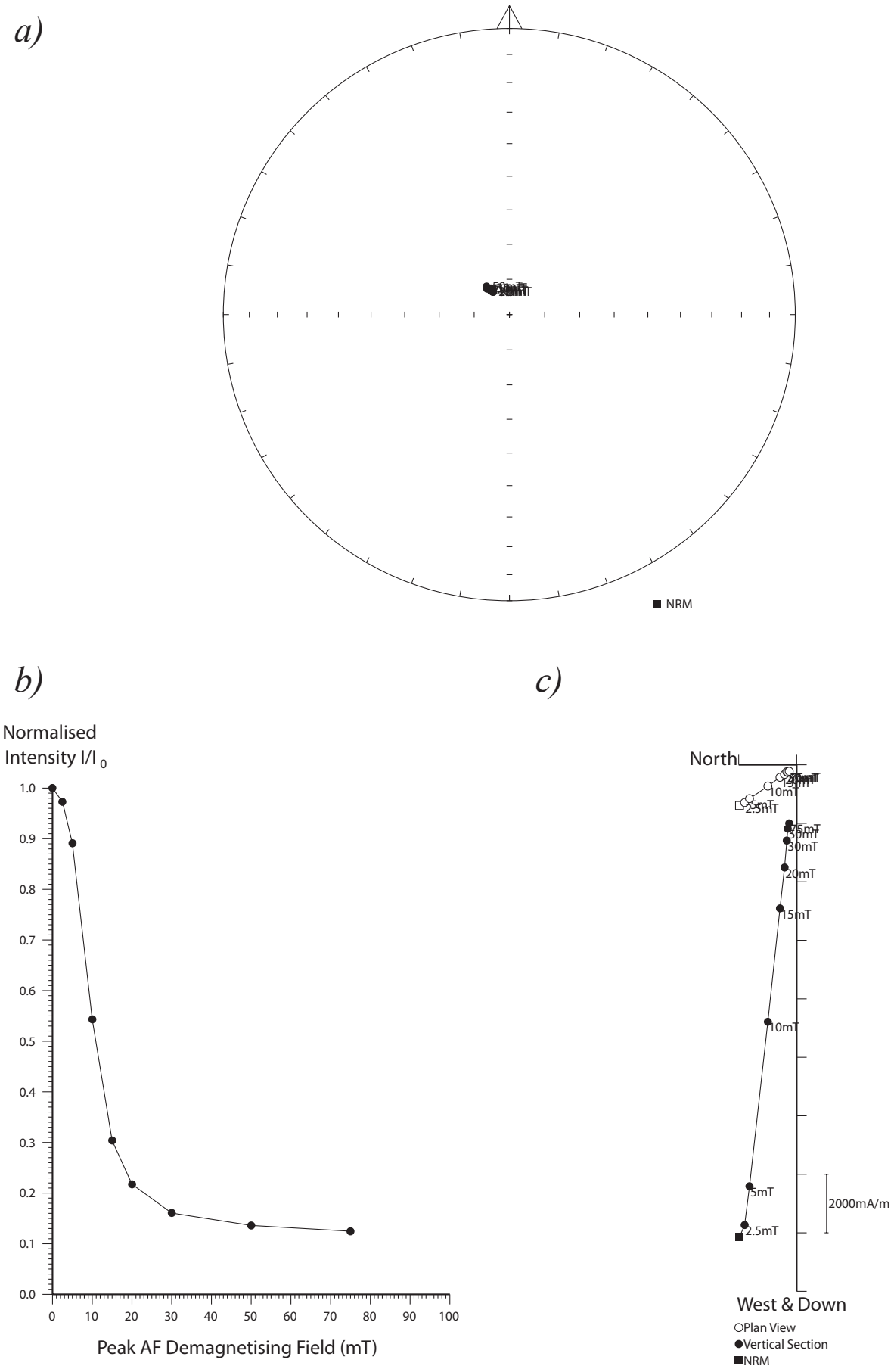

Figure 15: Stepwise AF demagnetisation of sample 3WB05. Diagram a) depicts the variation of the remanent direction as an equal area stereogram (declination increases clockwise, while inclination increases from zero at the equator to 90 degrees at the centre of the projection); b) shows the normalised change in remanence intensity as a function of the demagnetising field; c) shows the changes in both direction and intensity as a vector endpoint projection.

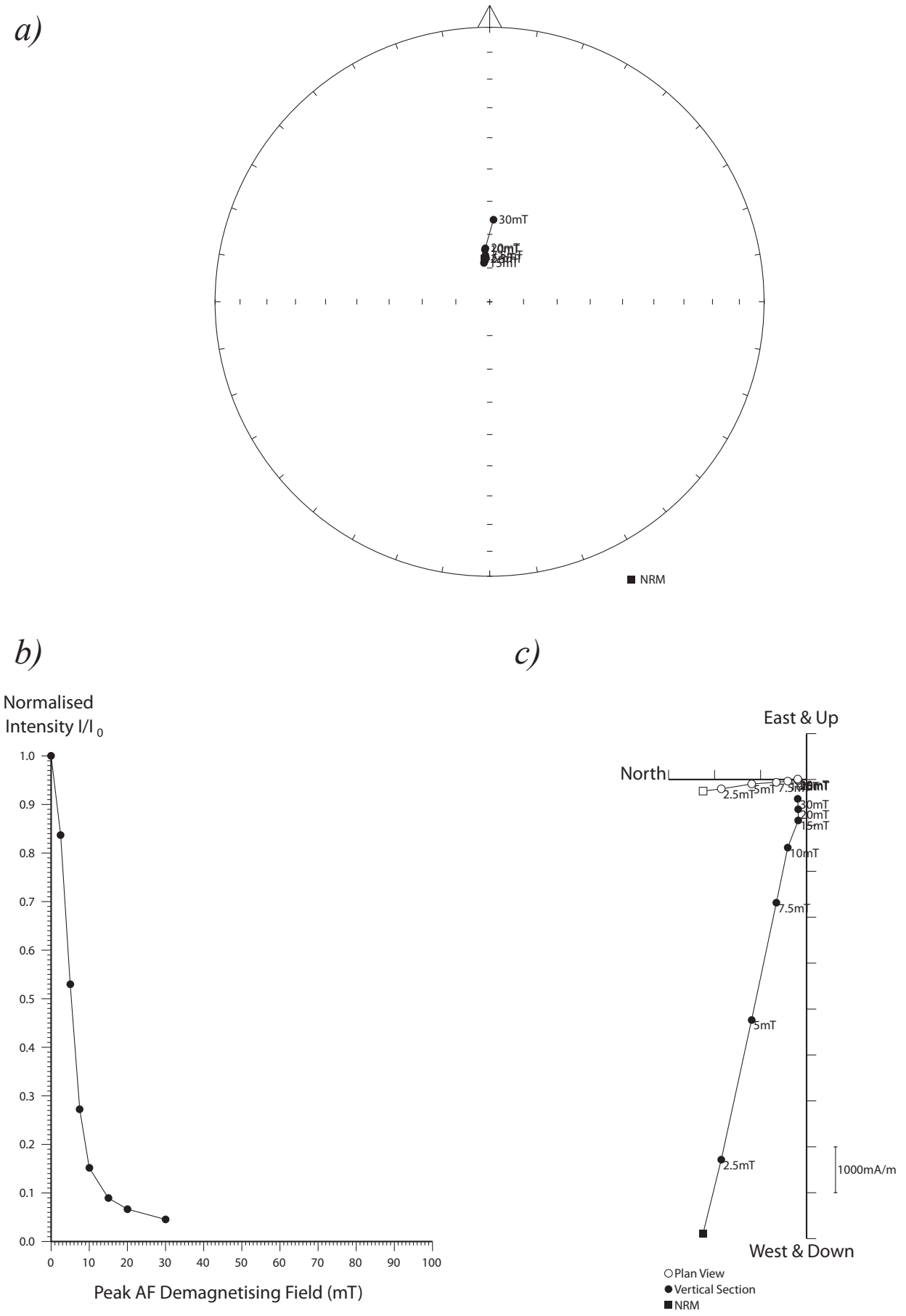

Figure 16: Stepwise AF demagnetisation of sample 1WB10. Diagram a) depicts the variation of the remanent direction as an equal area stereogram (declination increases clockwise, while inclination increases from zero at the equator to 90 degrees at the centre of the projection); b) shows the normalised change in remanence intensity as a function of the demagnetising field; c) shows the changes in both direction and intensity as a vector endpoint projection.

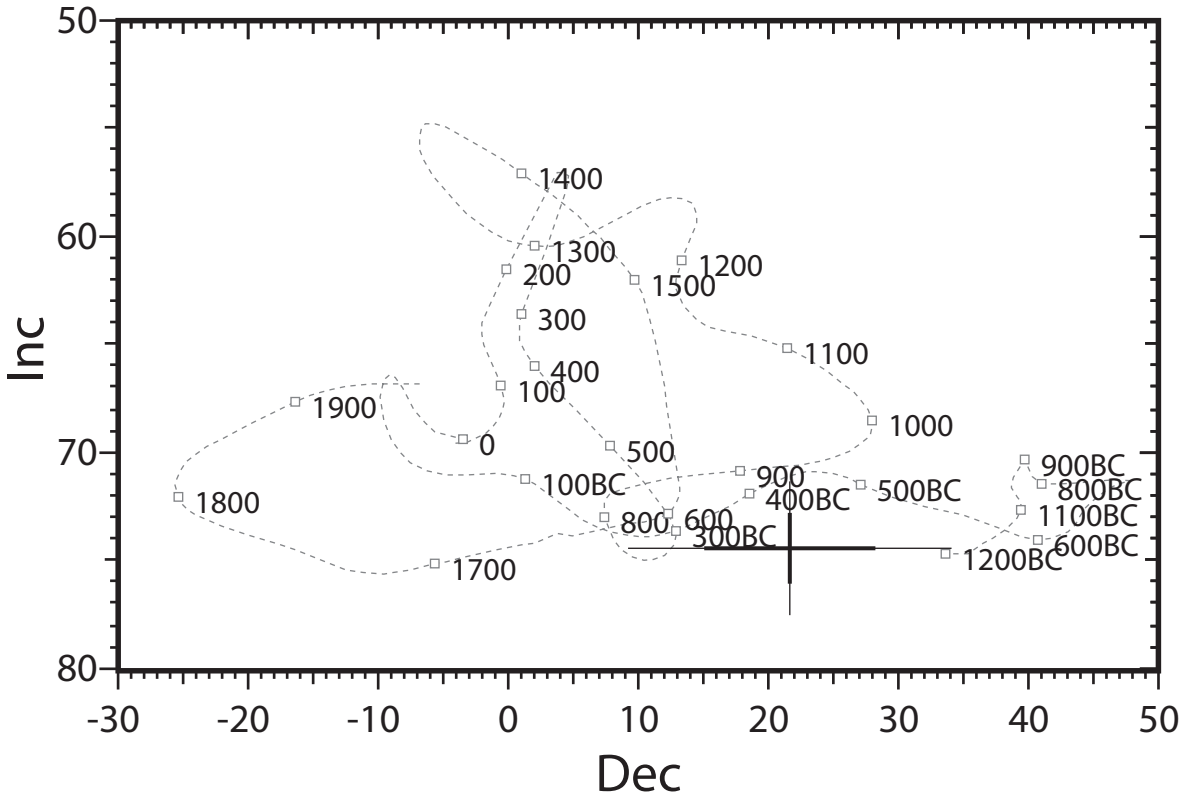

Figure 17: Comparison of the mean thermoremanent vector of samples 3WB01, 3WB03, 3WB06 and 3WB08-14 from feature 3WB after 5mT partial AF demagnetisation with the UK master calibration curve. Thick error bar lines represent 63% confidence limits and narrow lines 95% confidence limits.

a)

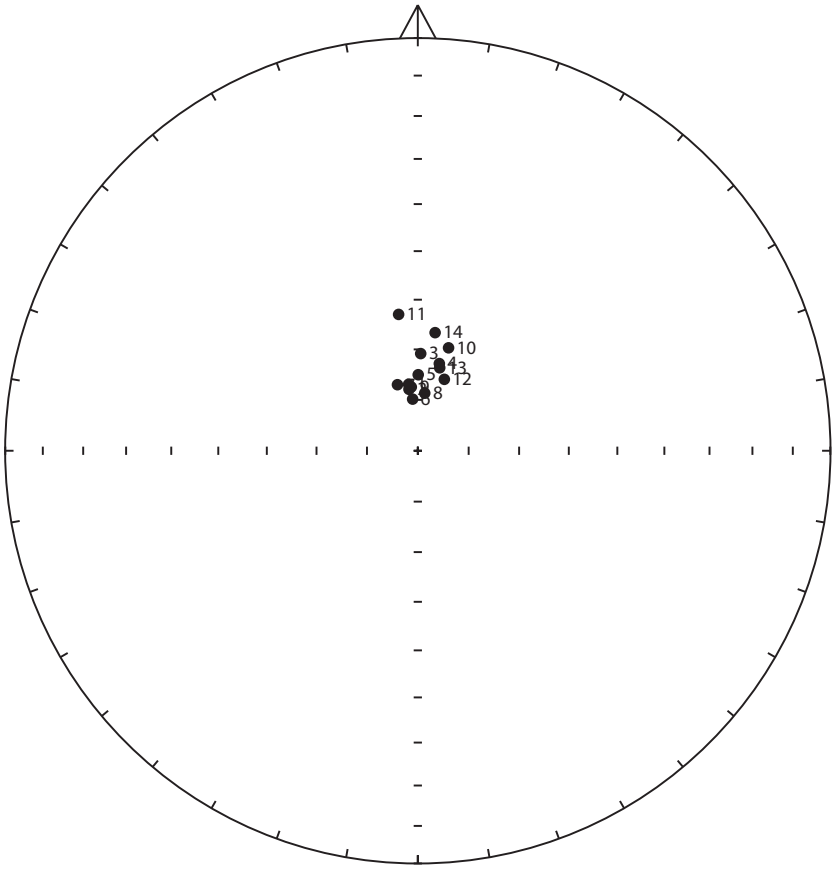

b)

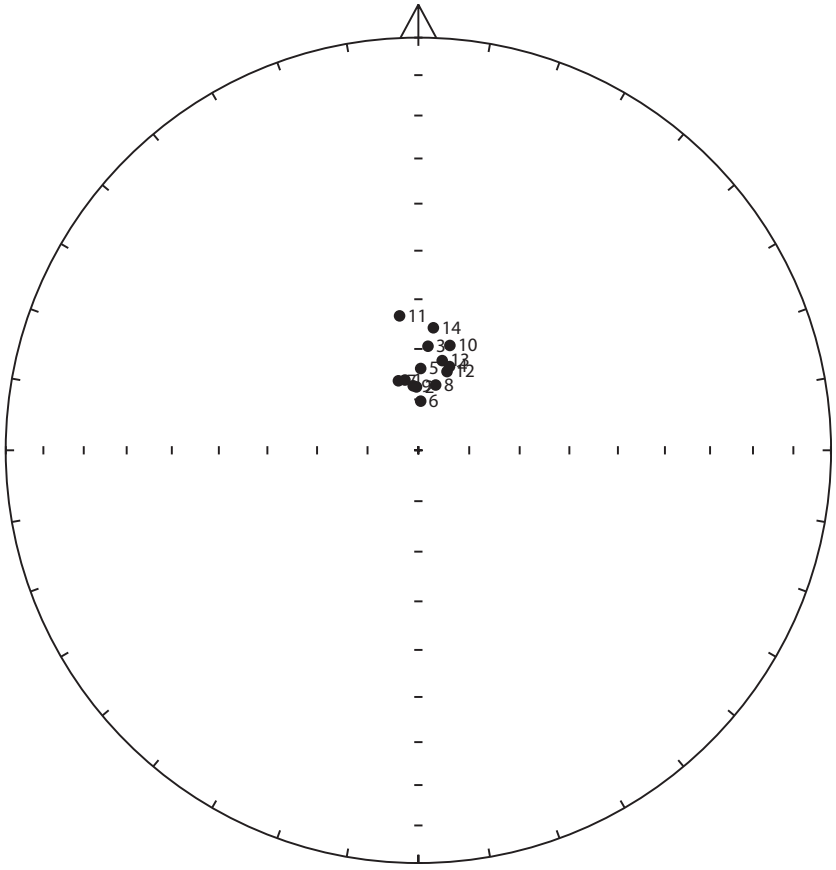

Figure 18: a) Distribution of NRM directions of samples from feature 4WB represented as an equal area stereogram. In this projection declination increases clockwise with zero being at 12 o'clock while inclination increases from zero at the equator to 90 degrees in the centre of the projection. Open circles represent negative inclinations. b) Distribution of thermoremanent directions of magnetisation of the same samples after partial AF demagnetisation to 5mT.

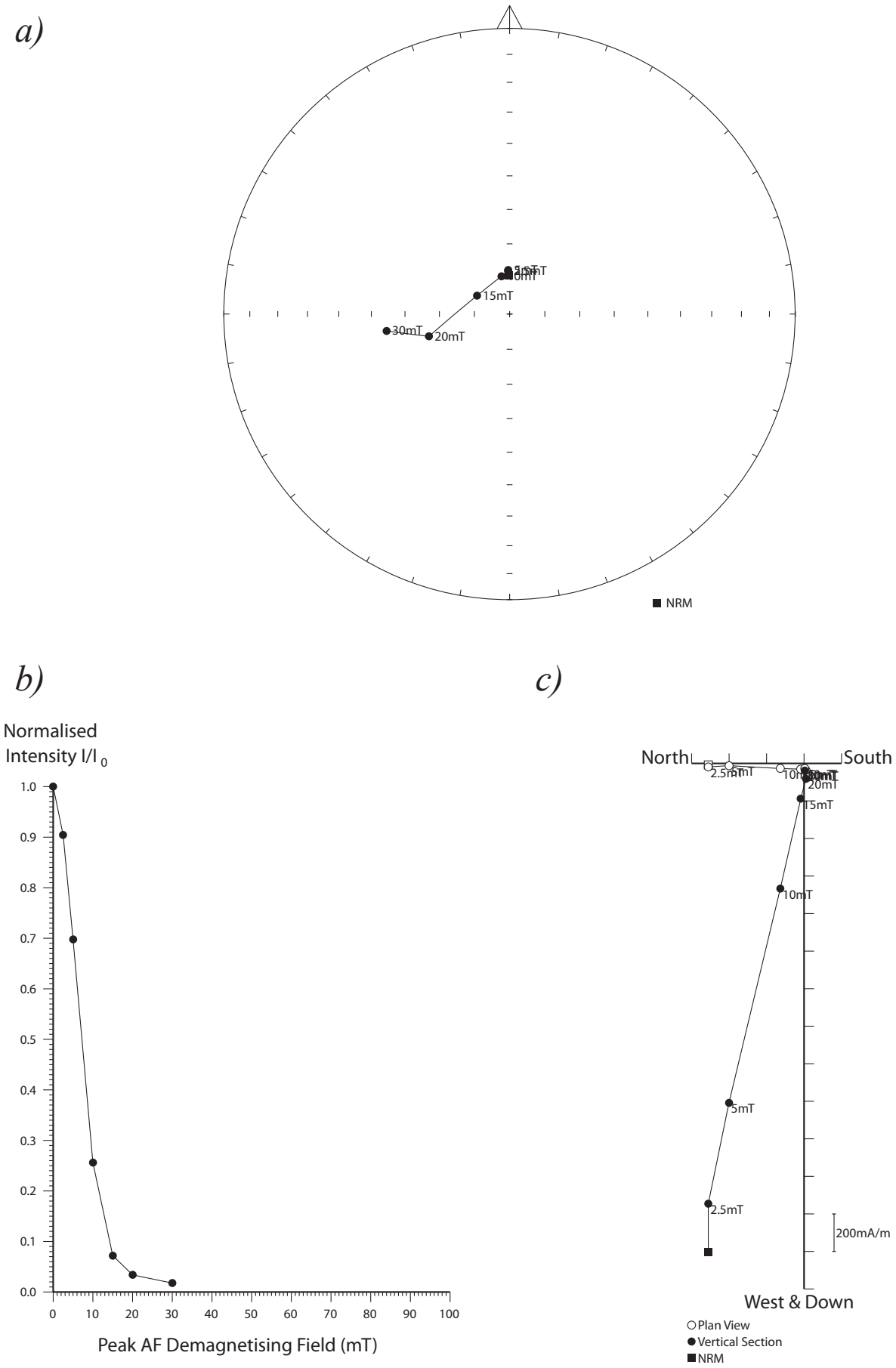

Figure 19: Stepwise AF demagnetisation of sample 4WB02. Diagram a) depicts the variation of the remanent direction as an equal area stereogram (declination increases clockwise, while inclination increases from zero at the equator to 90 degrees at the centre of the projection); b) shows the normalised change in remanence intensity as a function of the demagnetising field; c) shows the changes in both direction and intensity as a vector endpoint projection.

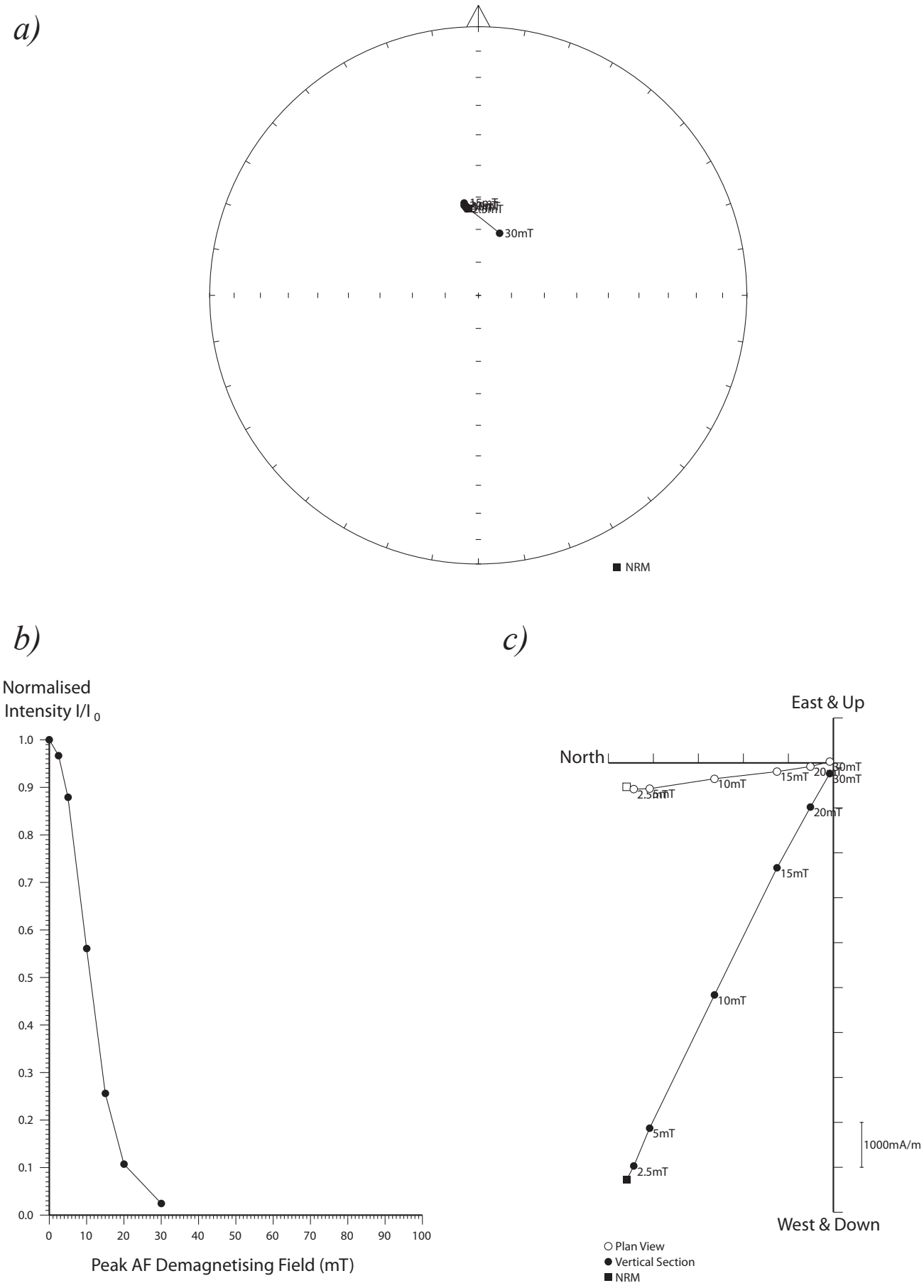

Figure 20: Stepwise AF demagnetisation of sample 4WB11. Diagram a) depicts the variation of the remanent direction as an equal area stereogram (declination increases clockwise, while inclination increases from zero at the equator to 90 degrees at the centre of the projection); b) shows the normalised change in remanence intensity as a function of the demagnetising field; c) shows the changes in both direction and intensity as a vector endpoint projection.

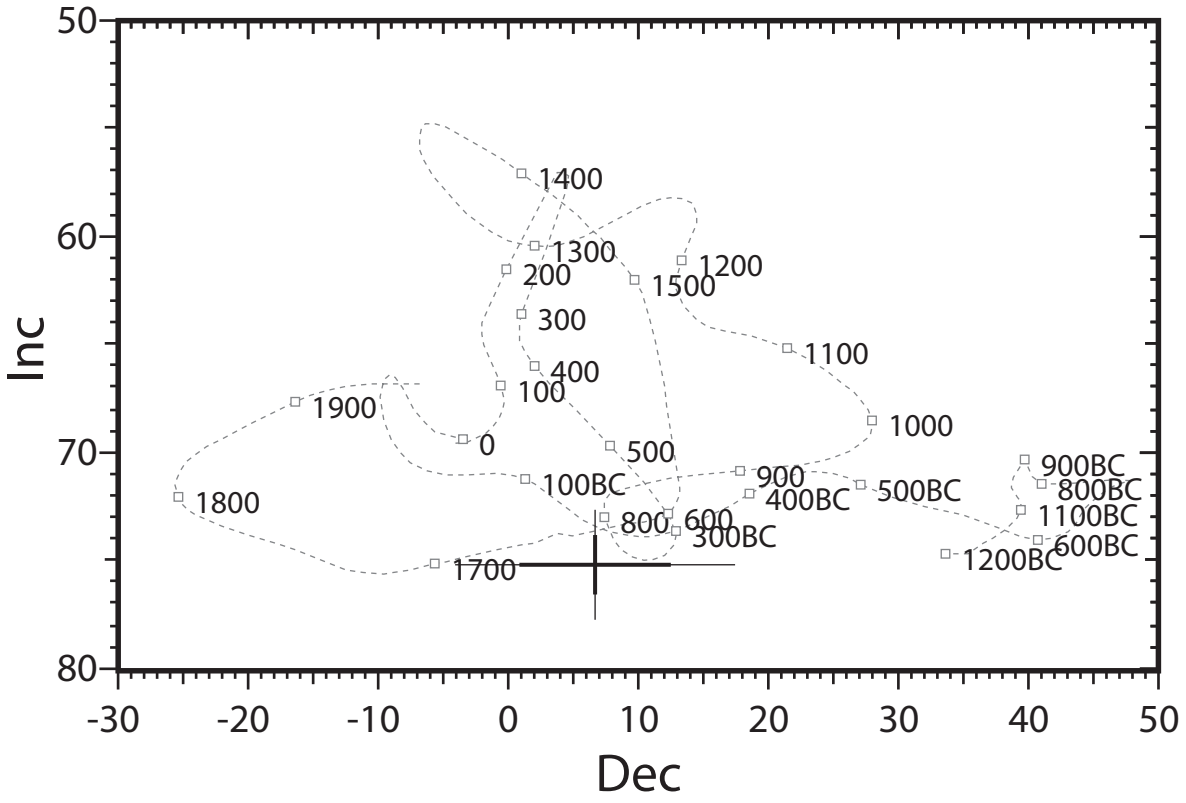

Figure 21: Comparison of the mean thermoremanent vector of samples 4WB01-10 and 4WB12-14 from feature 4WB after 5mT partial AF demagnetisation with the UK master calibration curve. Thick error bar lines represent 63% confidence limits and narrow lines 95% confidence limits.

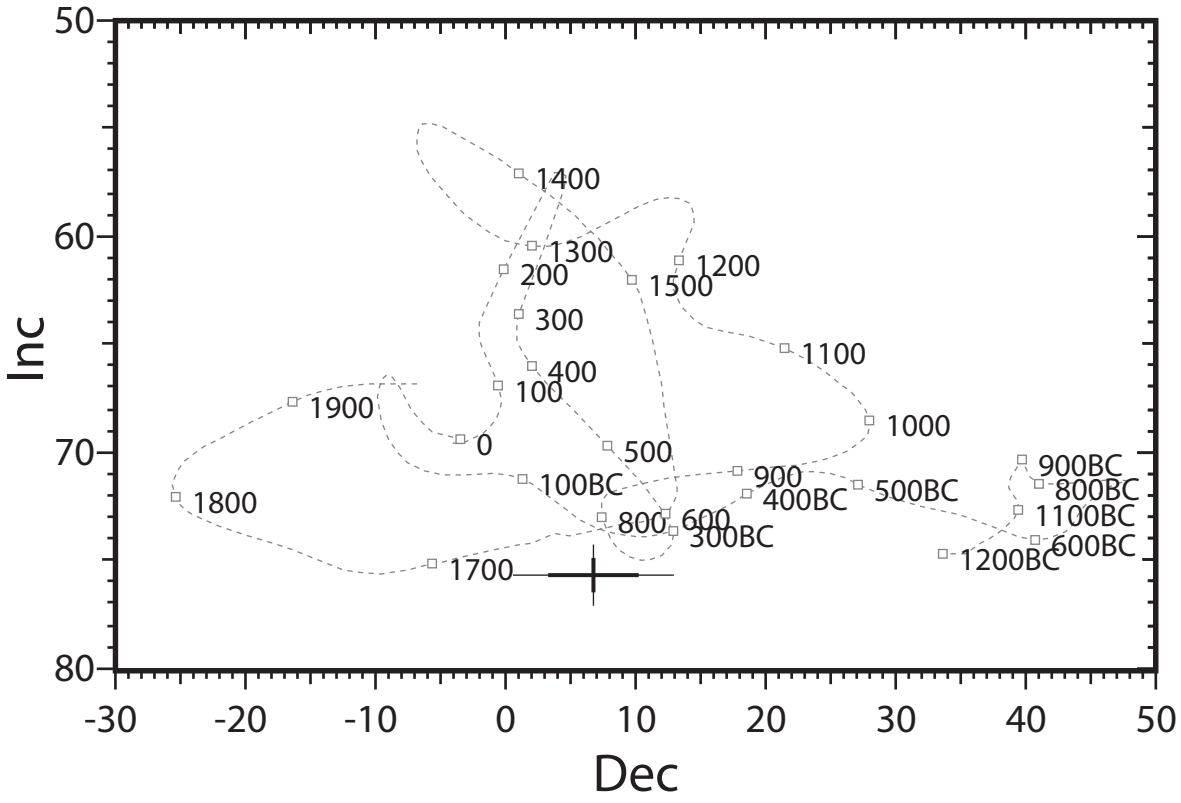

Figure 22: Comparison of the mean thermoremanent vector calculated using samples from both 1WB and 4WB with the UK master calibration curve. Thick error bar lines represent 63% confidence limits and narrow lines 95% confidence limits.